Activation of the Ca^{2+} sensing receptor and the PKC/WNK4 downstream signaling cascade induces incorporation of ZO-2 to tight junctions and its separation from 14-3-3

Elida Amaya[a], Lourdes Alarcón[a], Dolores Martín-Tapia[a], Francisco Cuellar-Pérez[a], Misael Cano-Cortina[a], Jose Mario Ortega-Olvera[a], Bulmaro Cisneros[b], Alexis J. Rodriguez[c], Gerardo Gamba[d,e,f], and Lorenza González-Mariscal[a,*]

[a]Center for Research and Advanced Studies (Cinvestav), Department of Physiology, Biophysics and Neuroscience, and [b]Department of Genetics and Molecular Biology, Mexico City 07360, Mexico; [c]Department of Biological Science, Rutgers, The State University of New Jersey, Newark, NJ 07102; [d]Molecular Physiology Unit, Instituto de Investigaciones Biomédicas, Universidad Nacional Autónoma de México, Mexico City 14080, México; [e]Department of Nephrology and Mineral Metabolism, Instituto Nacional de Ciencias Médicas y Nutrición Salvador Zubirán, Mexico City 14080, Mexico; [f]Tecnológico de Monterrey, Escuela de Medicina y Ciencias de la Salud, 64710 Monterrey, Nuevo Leon, México

ABSTRACT **Zonula occludens-2 (ZO-2) is a tight junction (TJ) cytoplasmic protein, whose localization varies according to cell density and Ca^{2+} in the media. In cells cultured in low calcium (LC), ZO-2 displays a diffuse cytoplasmic distribution, but activation of the Ca^{2+} sensing receptor (CaSR) with Gd^{3+} triggers the appearance of ZO-2 at the cell borders. CaSR downstream signaling involves activation of protein kinase C, which phosphorylates and activates with no lysine kinase-4 that phosphorylates ZO-2 inducing its concentration at TJs. In LC, ZO-2 is protected from degradation by association to 14-3-3 proteins. When monolayers are transferred to normal calcium, the complexes ZO-2/14-3-3ζ and ZO-2/14-3-3σ move to the cell borders and dissociate. The 14-3-3 proteins are then degraded in proteosomes, whereas ZO-2 integrates to TJs. From the plasma membrane residual ZO-2 is endocyted and degradaded in lysosomes. The unique region 2 of ZO-2, and S261 located within a nuclear localization signal, are critical for the interaction with 14-3-3 ζ and σ and for the efficient nuclear importation of ZO-2. These results explain the molecular mechanism through which extracellular Ca^{2+} triggers the appearance of ZO-2 at TJs in epithelial cells and reveal the novel interaction between ZO-2 and 14-3-3 proteins, which is critical for ZO-2 protection and intracellular traffic.**

Monitoring Editor
Asma Nusrat
University of Michigan

Received: Sep 20, 2018
Revised: Jul 6, 2019
Accepted: Jul 6, 2019

INTRODUCTION

Tight junctions (TJs) are cell–cell adhesion structures present at the upper portion of the lateral membrane of epithelial cells, which regulate the transit of ions and molecules through the paracellular space and maintain the polarized distribution of proteins and lipids between the apical and basolateral membranes (Mandel *et al.*, 1993). TJs are composed of a complex group of proteins including

This article was published online ahead of print in MBoC in Press (http://www.molbiolcell.org/cgi/doi/10.1091/mbc.E18-09-0591) on July 18, 2019.

*Address correspondence to: Lorenza González-Mariscal (lorenza@fisio.cinvestav.mx).

Abbreviations used: AICAR, 5-aminoimidazole-4-carboxamide riboside; AMPK, AMP-activated protein kinase; BBB, blood–brain barrier; bpNLS-2, bipartite nuclear localization signal 2; CaSR, Ca^{2+} sensing receptor; CS, calcium switch; DAG, diacylglycerol; DiC8, 1,2-dioctanoyl-*sn*-glycerol; DMSO, dimethyl sulfoxide; FCI, fluorescent covariance index; LC, low calcium; MDCK, Madin-Darby canine kidney; NC, normal calcium; NES, nuclear export signal; NLS, nuclear localization signal; PBS, phosphate-buffered saline; PCC, Pearson's correlation coefficient; PKC, protein kinase C; PLA, proximity ligation assay; pSer, phosphoserine; pThr, phosphothreonine; SS, steady state; TER, transepithelial electrical resistance; TJ, tight junction; U2, unique region 2; WNK, with no lysine kinase; WT, wild type; ZO-1, zonula occludens-1; ZO-2, zonula occludens-2.

transmembrane proteins such as claudins, junctional adhesion molecules, occludin, tricellulin and marvel-D3, and a vast array of cytoplasmic proteins that link the integral TJ proteins to the actomyosin cytoskeleton (Gonzalez-Mariscal, 2016a,b).

Zonula occludens-2 (ZO-2) is a cytoplasmic TJ protein of the MAGUK protein family (Gonzalez-Mariscal *et al.*, 2017) whose subcellular localization varies according to the confluence of the culture and the presence of calcium in the incubation media. Thus, in sparse cultures, ZO-2 is present at cell–cell contacts and the nuclei, while in confluent monolayers the protein concentrates at TJs. However, if confluent monolayers are incubated in low calcium (LC) media (1–5 μM), ZO-2 disappears from the cell borders and displays a diffuse cytoplasmic staining (Islas *et al.*, 2002).

The development of TJs requires the presence of extracellular Ca^{2+} (Cereijido *et al.*, 1981; Gonzalez-Mariscal *et al.*, 1990) and this process does not depend on an increase in cytosolic Ca^{2+}, as La^{3+} that impairs the influx of Ca^{2+} when cells are switched from LC to normal calcium (NC, 1.8 mM) media does not affect the sealing of TJs (Contreras *et al.*, 1992). The hypothesis that Ca^{2+} promotes TJ assembly by binding to a receptor molecule in the plasma membrane has been reinforced with the observation that in epithelial cells cultured in LC, the activation of the Ca^{2+} sensing receptor (CaSR), a G-protein-coupled receptor that codistributes with β-catenin on the basolateral membrane, induces the appearance of zonula occludens 1 (ZO-1) and occludin at cell–cell contact sites (Jouret *et al.*, 2013).

The 14-3-3 proteins, whose name makes reference to their migration pattern on two-dimensional DEAE-cellulose chromatography and starch gel electrophoresis, are small adaptor proteins with no enzyme activity that sequester proteins in the cytoplasm (for a review see Obsil and Obsilova, 2011). In this manner, 14-3-3 proteins prevent the degradation and regulate the intracellular traffic of their target proteins (Basu *et al.*, 2003; Zhao *et al.*, 2007). The 14-3-3 proteins bind to phosphoserine/phosphothreonine (pSer/pThr) residues in their targets present in the consensus R[S/Φ][+]pSXP or RX[Φ/S][+]pSXP (where pS is a phosphoserine, Φ is an aromatic residue, + is a basic residue, and X is any type of residue, typically Leu, Glu, Ala, and Met) (Yaffe *et al.*, 1997; Rittinger *et al.*, 1999). In mammals, seven 14-3-3 proteins, denoted as β, ε, η, γ, τ, ζ, and σ, have been identified. These proteins, although encoded by different genes, are commonly referred to as isoforms. The 14-3-3σ preferentially forms homodimers while the rest of the isoforms form both homo- and heterodimers (Wilker *et al.*, 2005). Mass spectrometry has revealed that ZO-2 binds to 14-3-3 α, γ, ζ (Jin *et al.*, 2004), θ (Wan *et al.*, 2015), and σ (Benzinger *et al.*, 2005) isoforms.

Here, we sought to analyze whether the activation of CaSR induces the recruitment of ZO-2 to the cell borders and the downstream signaling pathway involved. Then, we explore how ZO-2 is maintained in the cytoplasm in the LC condition, avoiding proteosomal degradation. Previously, we observed that if a Ca-switch (CS) was done in the presence of cycloheximide, an inhibitor of protein synthesis, the transepithelial electrical resistance (TER) developed, indicating that in the LC condition, TJ components were already synthesized even when TJs were not yet assembled (Gonzalez-Mariscal *et al.*, 1985). We analyzed whether ZO-2 associates to 14-3-3 proteins in the cytoplasm in the LC condition. Furthermore, we studied the association of ZO-2 with 14-3-3 isoforms σ and ζ and explored whether these interactions shield ZO-2 from degradation and regulate its intracellular traffic. We analyzed isoform 14-3-3σ because its expression is lost in numerous carcinomas (for a review see Khorrami *et al.*, 2017) and is known to restore cell polarity and to trigger the appearance of ZO-1 and E-cadherin at the cell borders of tumor cells (Ling *et al.*, 2010). Instead, 14-3-3ζ down-regulates 14-3-3σ expression (Xu *et al.*, 2015), its high abundance is associated with poor prognosis in several cancers (for a review see (Khorrami *et al.*, 2017)], and it exerts in several systems opposite roles to 14-3-3σ (Yang *et al.*, 2003; Lee and Lozano, 2006; Ling *et al.*, 2010), including the disruption of epithelial cell polarity (Hurd *et al.*, 2003).

RESULTS

Movement of ZO-2 from the cytoplasm to the cell borders is triggered by activation of the CaSR/ PKCε/ with no lysine kinase (WNK)4 signaling pathway

We tested whether Gd^{3+}, an agonist of CaSR, induced the movement of ZO-2 to the borders of Madin-Darby canine kidney (MDCK) cells cultured in LC media. In monolayers cultured for 24 h in NC media (steady state, SS), ZO-2 is present at the cell borders (Figure 1A), while in monolayers cultured in LC media and incubated for 2 h with dimethyl sulfoxide (DMSO) as vehicle, ZO-2 displays a diffuse cytoplasmic distribution (Figure 1B). In contrast, activation of CaSR with 100 μM Gd^{3+} triggers the appearance of discontinuous stretches of ZO-2 at the borders of cells cultured in LC media (Figure 1C).

CaSR signals through $G\alpha_i$ and $G\alpha_{q/11}$ subunits (for a review see Gonzalez-Mariscal *et al.*, 2018) and the latter activates phospholipase C that hydrolyzes phosphatidylinositol 4,5-biphosphate to diacylglycerol (DAG) and inositol triphosphate. The latter induces the release of Ca^{2+} from the endoplasmic reticulum, while DAG activates conventional and novel PKCs (cPKC, nPKC) (Davis *et al.*, 1985). Therefore, we tested whether permeable DAG, 1,2-dioctanoyl-*sn*-glycerol (DiC8), induced the appearance of ZO-2 at the border of cells cultured in LC, and in addition, we analyzed whether Gd^{3+} or DiC8 triggered the assembly at the cell borders of E-cadherin, a transmembrane protein of the adherens junction. We observed that while E-cadherin was not assembled at the cell periphery after Gd^{3+} or DiC8 treatment (Supplemental Figure S1), 0.5 mM of DiC8 induced the appearance of ZO-2 at cell–cell contacts (Figure 1E).

Then, we sought to identify the isoform of PKC involved in this process. Since bryostatin induces a rapid and sustained activation of isozymes δ and ε and only activates cPKCα after 3–4 h followed by down-regulation (Song *et al.*, 2001), we next incubated MDCK cells cultured in LC with 200 nM bryostatin and after 2 h observed the appearance of ZO-2 at the cell borders (Figure 1G), suggesting that either nPKC δ or ε were involved. To further distinguish between these isozymes, cells cultured in LC and preincubated for 30 min with 6 μM röttlerin that inhibits nPKCδ were then incubated for 2 h with Gd^{3+} under the continuous presence of röttlerin. Figure 1H shows the appearance of ZO-2 at the cell borders, thus indicating that nPKCδ is not required and that nPKCε can drive ZO-2 arrival to the cell border.

Next, we tested whether treatment with DiC8 increased the serine phosphorylation of ZO-2. For this purpose, we performed a proximity ligation assay (PLA) in monolayers cultured in LC and treated with DiC8 using antibodies against ZO-2 and pSer. Figure 2A shows an increase in red fluorescent dots in DiC8-treated monolayers, in comparison to monolayers maintained in LC medium, and reveals that PKC activation induced the phosphorylation of ZO-2 at serine residues at the same level as that achieved after a CS. To strengthen this observation, we also made an immunoprecipitation assay, observing that after DiC8 treatment, immunoprecipitated ZO-2 is more intensively phosphorylated in serine residues (Figure 2B).

Then, we analyzed whether PKC activation increased the phosphorylation of ZO-2 at PKC phosphorylation consensus sites in cells cultured in LC. For this purpose, cells cultured in LC were transfected with HA-cZO-2 and a PLA was done with an antibody against HA and a phospho-(Ser) PKC substrate antibody that binds to a

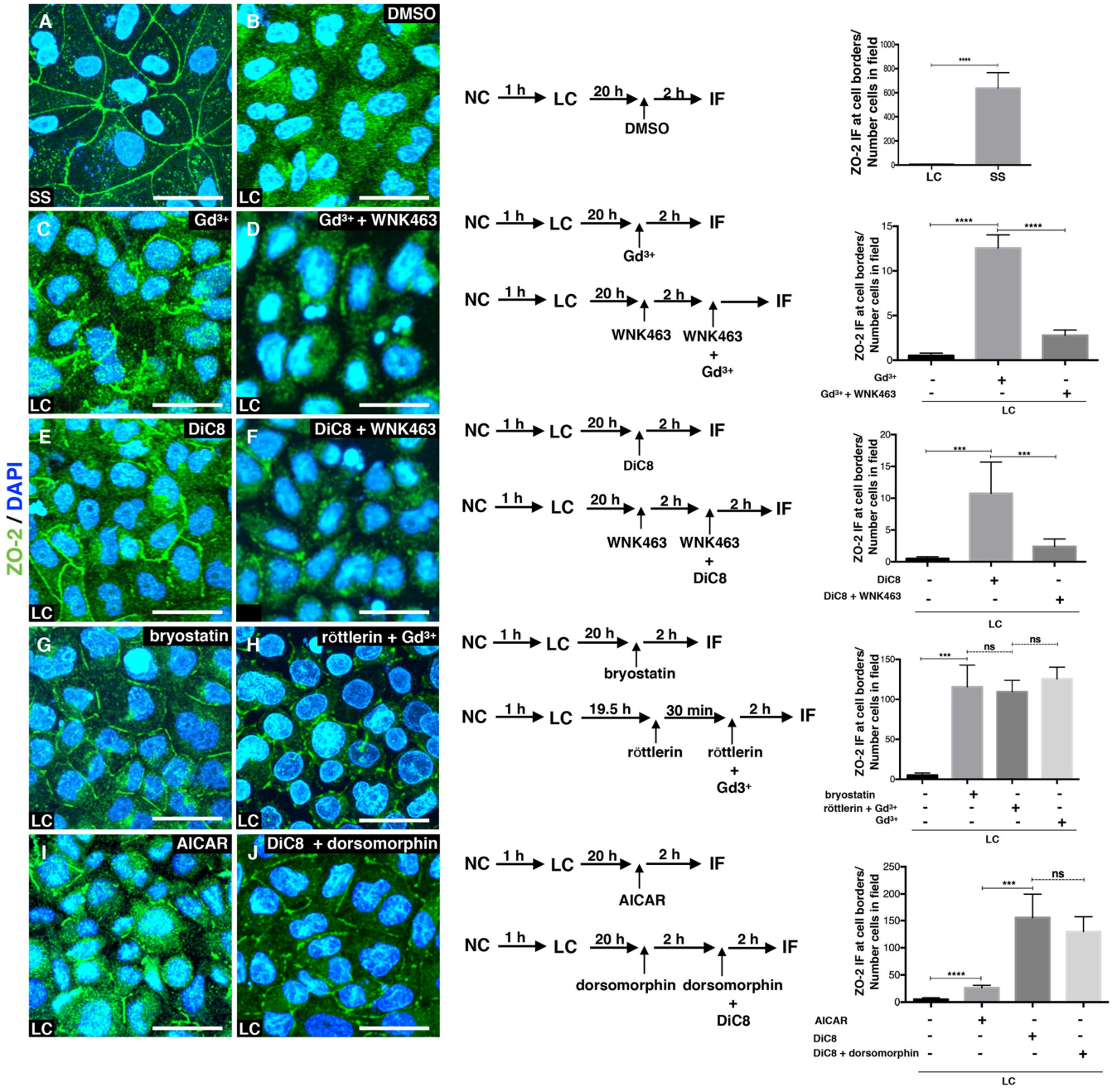

FIGURE 1: ZO-2 translocates to the cell borders on activation of the CaSR that through the $G\alpha_{q/11}$ subunit stimulates PKCε that in turn activates WNK proteins and adenylyl cyclase/AMPK. Monolayers were plated at confluent density and incubated in NC media for 24 h (SS) or for 1 h in NC media and then were transferred to LC for 20 h after which they were treated as indicated in the scheme, with 100 μM Gd^{3+}, an agonist of CaSR; 4 μM WNK463, an inhibitor of WNK proteins; 0.5 mM DiC8, an activator of conventional and novel PKCs; 200 nM bryostatin, an stimulator of nPKC δ and ε; 6 μM röttlerin an inhibitor of nPKCδ; 4 mM AICAR, a stimulator of AMPK; and 50 μM dorsomorphin, an inhibitor of AMPK. Left panels, immunofluorescence images done with an antibody against ZO-2. Nuclei were stained with DAPI. Bars, 20 μm. Images taken from at least two independent experiments. Middle panels, monolayer treatment scheme. Right panels, quantification of ZO-2 fluorescence staining at the cell borders. Statistical analysis was done with Student's *t* test ***$p < 0.001$; ****$p < 0.0001$; ns, nonsignificant. Results obtained from six optical fields in each experimental condition. Data are from two independent experiments. All the quantitative results in this and the following figures correspond to mean ± SE.

phosphorylated serine present in the consensus recognized by PKC: R/KXpSΦR/K (where X corresponds to any amino acid and Φ to a hydrophobic residue). Figure 2C shows that treatment of cells cultured in LC with DiC8 induces ZO-2 serine phosphorylation by cPKC/nPKC isoforms to the same level obtained with a CS.

In HEK-293 renal cells, CaSR activation and signaling through $G\alpha_{q/11}$ promote PKC-mediated phosphorylation and activation of WNK4 (Castaneda-Bueno *et al.*, 2017; Bazua-Valenti *et al.*, 2018). Hence, we asked whether the appearance of ZO-2 at the cell–cell borders induced by CaSR/$G\alpha_{q/11}$/PKC activation also involved the

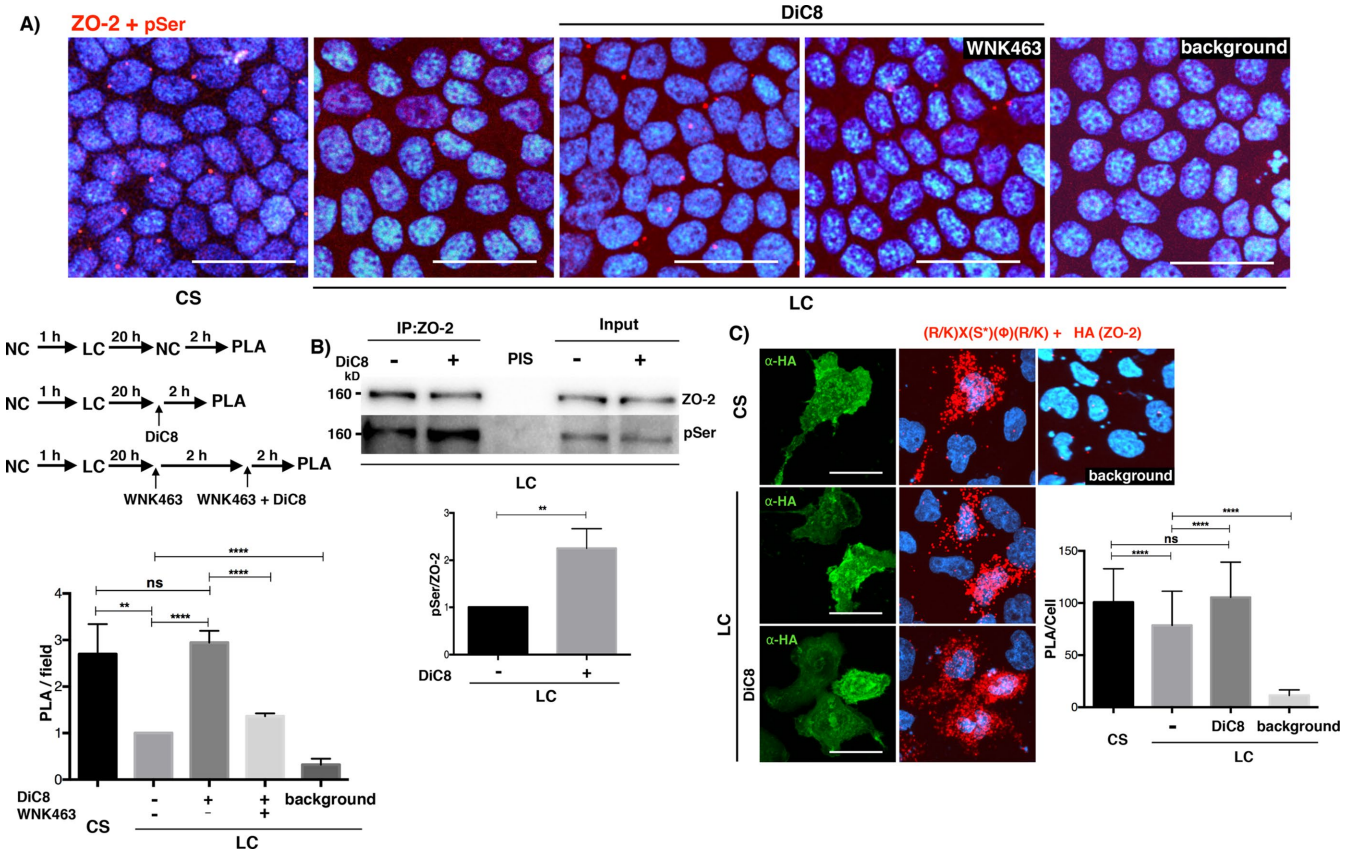

FIGURE 2: PKC activation increases the phosphorylation of ZO-2 at serine residues in monolayers cultured in LC media. (A) Monolayers cultured in LC for 20 h were subjected to a CS for 2 h or maintained in LC and treated or not (vehicle only, DMSO 0.25%) for 2 h with 0.5 mM DiC8, or pretreated for 2 h with 4 μM WNK463 and then transferred to media with 4 μM WNK463 plus 0.5 mM DiC8. The PLA was done with a rabbit antibody against ZO-2 and a mouse antibody anti pSer. Background, PLA done in LC monolayers without both primary antibodies. Nuclei stained with DAPI. Bar, 30 μm. Top panel, representative images; middle left panel, schematic design of experiment; bottom left panel, quantitative analysis done using BlobFinder. Statistical analysis done with one-way analysis of variance (ANOVA) followed by Dunnett's multiple comparison test, $^{**}p < 0.01$; $^{****}p < 0.0001$. Results were obtained from six optical fields in each experimental condition. Results are from two independent experiments. (B) The amount of phosphorylated serines residues in ZO-2 increased after DiC8 treatment. Western blot of a ZO-2 immunoprecipitate from LC cultured cells, treated or not for 2 h with 0.5 mM DiC8, and blotted against phosphorylated serine residues. Top panel, representative image of three independent experiments; bottom panel, quantitative analysis. Statistical analysis done with Student *t* test, $^{**}p < 0.01$. PIS, preimune serum. (C) MDCK monolayers were transfected with HA-cZO-2, cultured in LC for 20 h and then were subjected to a CS for 2 h or were maintained in LC and treated or not for 2 h with 0.5 mM DiC8. PLA was done with a rabbit antibody against phosphorylated serines present in the PKC target motif R/KXSφR/K and a mouse antibody anti HA. Cells transfected with HA-ZO-2 were identified with a mouse antibody anti HA, followed by a secondary goat anti-mouse IgG coupled to Alexa Fluor 488. Background corresponds to LC cultured cells not transfected with HA-cZO-2. Bars, 20 μm. Left panel, representative images; right panel, quantitative analysis done using BlobFinder. Statistical analysis done with one-way ANOVA followed by Dunnett's multiple comparison test $^{****}p < 0.0001$. Results obtained with 100 transfected cells per condition derived from two independent experiments.

subsequent activation of WNK4. Figure 1D shows that in LC media, ZO-2 relocation to the cell borders triggered by CaSR activation with Gd^{3+} is prevented by treatment with the specific inhibitor of WNK proteins WNK463 (Yamada *et al.*, 2016). Furthermore, Figure 1F shows that in cells cultured in LC the movement of ZO-2 to the cell borders after PKC stimulation with DiC8 is blocked on treatment with WNK463. Altogether these results indicate that the appearance of ZO-2 at the plasma membrane is triggered by extracellular Ca^{2+} that activates the CaSR, which in turn signals through $G\alpha_{q/11}$ promoting the subsequent activation of PKC and WNK proteins.

Next, we tested whether WNK4 binds to ZO-2 and whether this interaction increased after PKC activation. For this purpose, MDCK cells cultured in LC were transfected with a WNK4-HA construct and treated with DiC8 or bryostatin. Then, a PLA was done with a rabbit antibody against ZO-2 and a mouse antibody anti HA, showing that the interaction between WNK4 and ZO-2 augments on activation of cPKC and nPKC with DiC8 (Figure 3A, a and a'), and after the activation of nPKC δ and ε with bryostatin (Figure 3A, b and b'), the latter to a level similar to that observed after a CS (Figure 3A, d and d').

To further confirm the importance of PKCε activation for WNK4/ZO-2 interaction, we made the same PLA assay but after pretreating the cells with the following PKC inhibitors: 25 mM Ro 31-8220 that inhibits cPKC βI, βII, and nPKC ε (Wilkinson *et al.*, 1993) and the PKCε permeable inhibitor peptide εv1-2 (Liedtke *et al.*, 2002). These treatments obliterate the appearance of the red fluorescent spots that indicate WNK4/ZO-2 interaction after DiC8 or bryostatin

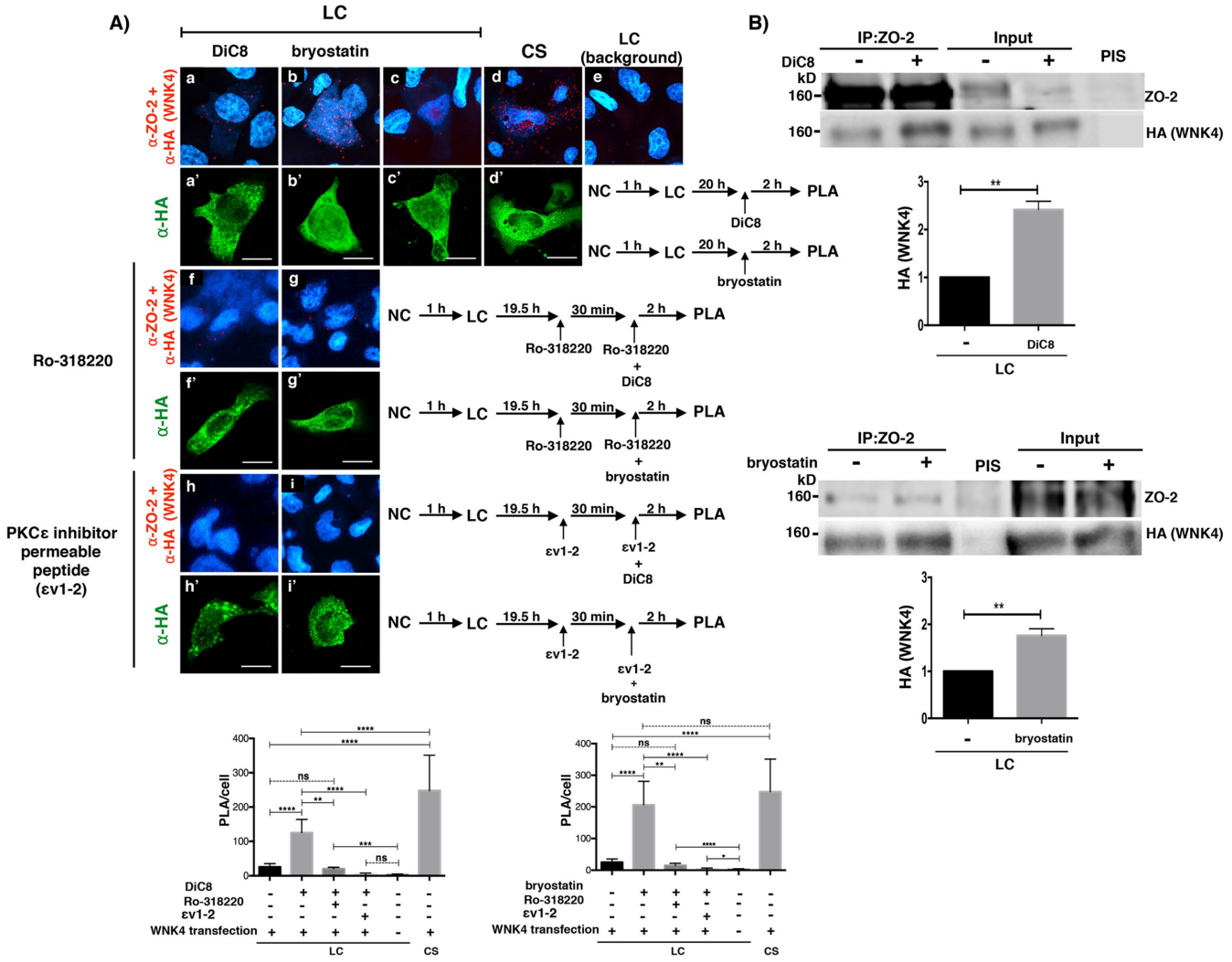

FIGURE 3: PKCε activation increases the interaction of ZO-2 with WNK4 in monolayers cultured in LC media. (A) PLA assays done in monolayers cultured in LC or after a CS with a rabbit antibody against ZO-2 and a mouse antibody anti-HA. Monolayers were treated or not for 2 h with 0.5 mM DiC8 or 200 nM bryostatin. In addition, as indicated, some monolayers were pretreated for 30 min and thereafter for 2 h with 25 nM Ro-318220, or 2 μM of the PKCε inhibitor permeable peptide εv1-2. Cells transfected with WNK4-HA were identified with a mouse antibody anti HA, followed by a secondary goat anti-mouse IgG coupled to Alexa Fluor 488. Background corresponds to LC cultured cells not transfected with WNK4-HA. Bars, 25 μm. Top panel, representative images; bottom panel, quantitative analysis done using BlobFinder. Statistical analysis was done with Kruskal-Wallis test followed by Dunn's multiple comparison test, $*p < 0.05$; $**p < 0.01$; $***p < 0.001$; $****p < 0.0001$; ns, nonsignificant. Results obtained from 30 transfected cells per condition derived from two independent experiments. (B) Treatment with DiC8 or bryostatin augments the amount of WNK4 that coimmunoprecipitates with ZO-2. ZO-2 was immunoprecipitated from LC cultured cells transfected with a WNK4-HA construct and treated or not for 2 h with 0.5 mM DiC8 or 200 nM bryostatin. After the SDS–PAGE the resulting membranes were blotted against HA and ZO-2. Results are from three independent experiments. Statistical analysis done with one-way ANOVA followed by Dunnett's multiple comparison test, $**p < 0.01$.

treatment (Figure 3A, f, f′, g, g′, h, h′, i, and i′), thus confirming the importance of PKCε activation to induce WNK4/ZO-2 interaction.

To further strengthen our results, we immunoprecipitated ZO-2 from LC cultured cells transfected with a WNK4-HA construct and blotted against HA, and observe that treatment with DiC8 or bryostatin augments the amount of WNK4 that coimmunoprecipitates with ZO-2 (Figure 3B), thus confirming that PKC activation promotes WNK4/ZO-2 interaction.

Then, we explored whether PKC activation promotes ZO-2 phosphorylation by WNK in LC-cultured cells. For this purpose, MDCK cells cultured in LC were treated with DiC8 with and without the WNK inhibitor WNK463. The PLA in Figure 2A revealed that inhibition of WNK enzymes reduced serine phosphorylation in ZO-2 triggered by PKC activation.

Altogether these results indicate that activation of the CaSR stimulates the $G_{q/11}$ pathway that induces the activity of PKCε, which in turn phosphorylates ZO-2 and WNK4, leading to further serine phosphorylation of ZO-2 and the movement of this protein to the cell borders.

Activation of adenylyl cylase by PKC is not required for the movement of ZO-2 to the cell borders in cells cultured in LC

AMP-activated protein kinase (AMPK) is a serine/threonine protein kinase that senses the energy status in eukaryotic cells (for a review

see Gowans and Hardie, 2014). AMPK is activated during calcium-induced TJ assembly and in cells cultured in LC, AMPK activation by 5-aminoimidazole-4-carboxamide ribonucleoside (AICAR), relocates ZO-1 to the cell borders (Zhang *et al.*, 2006). Here we observe that ZO-2 also relocates to cell–cell contacts in monolayers cultured in LC on treatment with AICAR, albeit with less intensity than with DiC8 treatment (Figure 1I). Since PKC (Zimmermann and Taussig, 1996; Kawabe *et al.*, 1994) and its activation with phorbol esters stimulates adenylyl cyclase activity (Jacobowitz *et al.*, 1993; Yoshimura and Cooper, 1993), and forskolin, a stimulator of adenylyl cyclase induces AMPK activation (Egawa *et al.*, 2008), we next tested whether the arrival of ZO-2 to the cell borders triggered by DiC8 in monolayers cultured in LC could be blocked by the inhibition of AMPK with dorsomorphin. Figure 1J shows that this is not the case, thus indicating that the appearance of ZO-2 at the cell borders triggered by CaSR activation and PKC signaling does not require the indirect activation of AMPK.

14-3-3 sequesters ZO-2 in cells incubated in LC media

We explored how ZO-2 could be maintained in the cytoplasm of cells cultured in LC, by focusing on the interaction of ZO-2 with 14-3-3. For this purpose, we performed an in silico search of putative 14-3-3 binding sites present in ZO-2 sequence (Scansite, http://scansite.mit.edu/ and 14-3-3-Pred, www.compbio.dundee.ac.uk/1433pred/) and found 25 and 22 sites in canine and human ZO-2, respectively (Supplemental Table 1 and Figure 4A). Next, we tested whether the cytoplasmic distribution of ZO-2 changed after treatment with BV02, a nonpeptidic inhibitor of 14-3-3 (Mancini *et al.*, 2011). Figure 4B (first column) shows that the addition of BV02 induced the appearance of ZO-2 at the cell border in the LC condition. These results hence suggested that in the LC condition, 14-3-3 sequesters ZO-2 inhibiting its appearance at the cell borders. Then, we observed by Western blot that inhibition of 14-3-3 with BV02 decreased ZO-2 level and that treatment with MG132, a peptide aldehyde that inhibits the proteosome (for a review see Lee and Goldberg, 1998), significantly increases the amount of ZO-2 present in the LC condition, irrespective of BV02 treatment (Figure 4C). These results suggested that in the LC condition, a considerable amount of Z0-2 is degraded in the proteasome, while a portion of ZO-2 is maintained sequestered by 14-3-3. To further confirm that inhibition of 14-3-3 with BV02 promotes proteosomal degradation of ZO-2, we transfected MDCK cells cultured in LC condition with a HA-ubiquitin construct, treated the monolayers with BV02 and MG132, and immunoprecipitated ZO-2. Figure 4D reveals that the amount of ubiquitin in the immunoprecipitated ZO-2 from LC cultured cells increased after inhibition of the proteasome with MG132. In addition, ubiquitinated ZO-2 also augments on treatment with BVO2, thus suggesting that the interaction of 14-3-3 with ZO-2 protects ZO-2 from proteosomal degradation.

Next, we analyzed the turnover rate of ZO-2 in monolayers cultured in LC and found that the half-life of ZO-2 diminishes to 7 h in the LC condition in comparison to the 19.7 h observed in NC (Supplemental Figure S2). This result hence suggests that in the LC condition where TJ are not established, ZO-2 is unstable and is constantly degraded.

Then, we analyzed by Western blot whether the subcellular distribution of ZO-2 changed after BV02 treatment using a cell fractionation assay in MDCK cells cultured in LC condition. Figure 4E shows that irrespective of BV02 treatment, ZO-2 in the LC condition mainly concentrates at the nucleus, while the amount found in the membrane and cytoplasm is barely detectable by Western blot. We had previously shown that the nucleus acts as a cellular ZO-2 reservoir and that the amount of ZO-2 at the membrane is significantly lower and is maintained relatively constant (Chamorro *et al.*, 2009). In this fractionation assay, we also observed a decrease in the amount of ZO-2 triggered by BV02 that mainly corresponds to changes in nuclear Z0-2 content. In addition, we found that in the LC condition the amount of ZO-2 present at the plasma membrane is very low, and that BV02 treatment further reduces this amount. Therefore, the appearance of ZO-2 at the cell border of LC-cultured cells, triggered by BVO2, could be explained not by ZO-2 recruitment to the cell borders but by the detachment of ZO-2 from 14-3-3 that might allow ZO-2 to polymerize, facilitating its observation at the cell borders by immunofluorescence.

Since ZO-2 through its second PDZ domains forms homodimers with itself and heterodimers with ZO-1 (Itoh *et al.*, 1999; Utepbergenov *et al.*, 2006; Chen *et al.*, 2009), we asked whether treatment with BV02 could also induce the appearance of ZO-1 at the cell borders in the LC condition. Figure 4B reveals by immunofluorescence the appearance of ZO-1 at the plasma membrane, while no recruitment of the integral TJ proteins occludin and claudin-1, or the peripheral TJ protein cingulin, was observed (Figure 4B).

The interaction of ZO-2 with 14-3-3 σ and ζ observed in the LC condition diminishes after CS or after activation of the CaSR/PKCε signaling pathway

Next, we explored the interaction of ZO-2 with 14-3-3 in the LC and CS condition. For this purpose, we immunoprecipitated ZO-2 and blotted with an antibody against pan14-3-3, finding that the coimmunoprecipitated 14-3-3 diminished after the CS in comparison to the LC condition (Figure 5A). To test the in situ interaction between ZO-2 and 14-3-3, we performed a PLA with a rabbit antibody against ZO-2 and a mouse antibody anti pan14-3-3. Positive red fluorescent spots appeared in MDCK cells cultured in LC, revealing that ZO-2 and 14-3-3 interact in the cytoplasm. However, the number of red spots diminished 4 h after CS (Figure 5B).

As 14-3-3 interacts with phosphorylated residues in its target proteins, we then tested whether inhibition of PKCδ with 6 μM röttlerin had an impact on the association of 14-3-3 with ZO-2. A PLA done with antibodies against ZO-2 and pan14-3-3 revealed that the interaction between these proteins requires the activity of PKCδ, since treatment with röttlerin inhibits the appearance of the fluorescent red spots (Figure 5C).

Then, we analyzed in dual-color confocal images the colocalization of isoforms 14-3-3σ and 14-3-3ζ with ZO-2 before and after CS and in cells cultured in NC for 24 h (SS). In the LC condition, both isoforms colocalize with ZO-2 in the cytoplasm (merge, yellow staining); in contrast, a faint colocalization was observed in the SS condition (Figures 6A and 7A). With time after CS, the cytoplasmic colocalization diminishes and ZO-2 concentrates at the cell borders, while the signal of 14-3-3σ and 14-3-3ζ decreases and remains scattered in the cytoplasm. Next, we employed Pearson's correlation coefficient (PCC), a statistic for quantifying colocalization that is independent of signal levels and signal background (Dunn *et al.*, 2011). PCC values range from 1 for two images whose fluorescence intensities are perfectly related to –1 for two images whose fluorescence intensities are inversely related to one another, and values near 0 indicate distribution of probes that are uncorrelated with one another. Thus, the right panels of Figures 6A and 7A demonstrate that the colocalization of 14-3-3σ and 14-3-3ζ with ZO-2 in the cytoplasm is high in the LC condition and diminishes after the CS. Then, we derived a covariance measure, named Fluorescence covariance index (FCI = Log10 of PCC at cell periphery/PCC at cytoplasm) to compare the colocalization of 14-3-3σ and

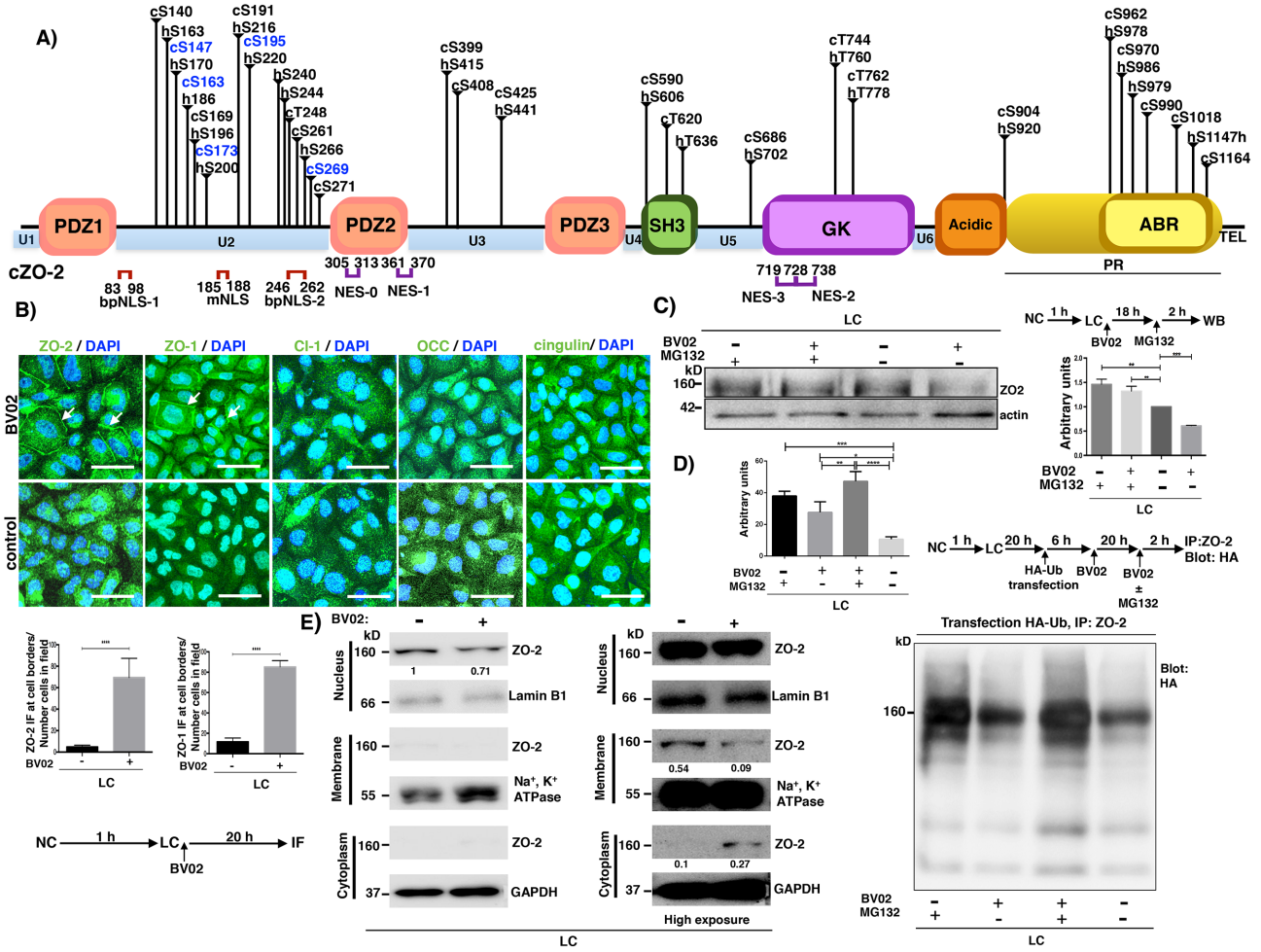

FIGURE 4: ZO-2 is sequestered in the cytoplasm by 14-3-3 in the LC condition. (A) cZO-2 and hZO-2 sequences, respectively, have 25 and 22 putative 14-3-3 binding sites, 11 (cZO-2) and 10 (hZO-2) of which are located at the U2 segment. Scheme showing the molecular organization of ZO-2. PDZ, PDZ domain; SH3, Src homologous 3 domain; GK, guanylate kinase domain; Acidic, acidic region; PR, proline-rich segment; ABR, actin binding region; U, unique region; TEL, PDZ binding motif; NLS, nuclear localization signal; NES, nuclear exportation signal; vertical lines, putative 14-3-3 binding sites; blue letters and numbers, putative 14-3-3 binding sites located within an SR motif. (B) The inhibition of 14-3-3 with BV02 induces the appearance of ZO-1 and ZO-2 at the cell borders of cells cultured in LC. MDCK cells were plated at confluent density in NC media and after 1 h were washed 5× with PBS without Ca^{2+} and transferred to LC media with 50 μM BV02 or vehicle only (DMSO 0.25%, control). After 20 h the monolayers were fixed and processed for immunofluorescence with antibodies against ZO-1, ZO-2, claudin-1, occludin, and cingulin. Top panel, representative images from three independent experiments. Nuclei were stained in blue with DAPI. Bar, 25 μm. Bottom panel, quantification of ZO-1 and ZO-2 fluorescence staining at the cell borders. Statistical analysis done with Student's *t* test, $^{****}p < 0.0001$. Results obtained from six optical fields in each experimental condition. (C) The cellular content of ZO-2 diminishes in the LC condition after the inhibition of 14-3-3 with BV02, due to protein degradation in the proteosome. Cell lysates were obtained from monolayers cultured in the LC condition for 18 h in the presence or absence of 50 μM BV02 and then were incubated or not for 2 h with 30 μM MG132. Top panel, representative Western blot; bottom panel, densitometric analysis. Statistical analysis done with one-way ANOVA followed by Dunnett's multiple comparison test, $^{**}p < 0.05$; $^{***}p < 0.01$. Results were obtained from three independent experiments. (D) Inhibition of 14-3-3 with BV02 promotes ubiquitination of ZO-2. MDCK cells cultured in LC condition for 20 h were transfected with a HA-ubiquitin construct. After 6 h, the monolayers were incubated with 50 μM BV02 for 20 h. In some monolayers, 30 μM of MG132 was also present in the last 2 h of incubation. ZO-2 was immunoprecipitated with a specific antibody and the blot was done with an antibody against HA. Top left panel, densitometric analysis. Statistical analysis was done with one-way ANOVA followed by Bonferroni's multiple comparison test, $^{*}p < 0.005$; $^{**}p < 0.01$; $^{***}p < 0.001$; $^{****}p < 0.0001$. Results were obtained from three independent experiments. Bottom right panel, representative Western blot. (E) The amount of ZO-2 in the plasma membrane of cells cultured in LC decreases after 14-3-3 inhibition. Western blot of nuclear, membrane, and cytoplasm fractions derived from LC cultured cells treated for 20 h with 50 μM BV02. Antibodies against lamin B1, Na^+,K^+-ATPase β1 subunit, and GAPDH were employed as markers of nuclear, plasma membrane, and cytoplasmic fractions, respectively. Numbers below the bands correspond to densitometric values reported as a ratio of ZO-2/lamin B1 in the nuclear fraction; ZO-2/Na^+, K^+, ATPase in the membrane fraction; and ZO-2/ GAPDH in the cytoplasm fraction of this representative experiment of a set of two independent experiments.

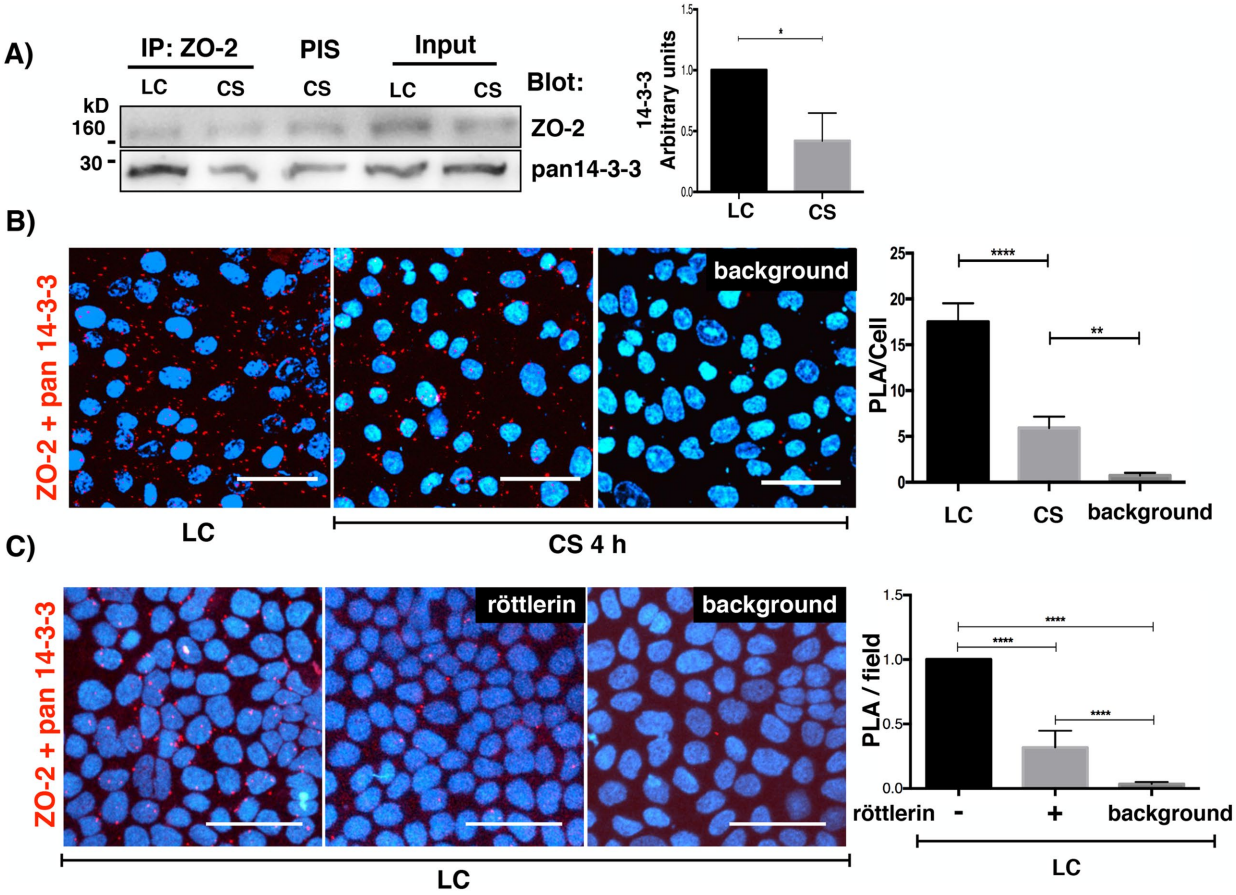

FIGURE 5: ZO-2 interacts in the cytoplasm with 14-3-3 in monolayers cultured in LC and this interaction diminishes with the CS. (A) The amount of 14-3-3 that coimmunoprecipitates with ZO-2 diminished after the CS. ZO-2 was immunoprecipitated from monolayers cultured in LC, and after a 4-h CS with a specific antibody, and the membranes were blotted with antibodies against ZO-2 and pan 14-3-3. PIS, preimmune serum. Left panel, representative image of three independent experiments; right panel, quantitative analysis. Statistical analysis was done with Student's *t* test; *$p < 0.05$. (B) ZO-2 interaction with 14-3-3 in the cytoplasm of LC cultured cells diminishes with the CS. PLA was done in monolayers cultured in LC and after a 4-h CS with a rabbit antibody against ZO-2 and a mouse antibody anti pan 14-3-3. Nuclei were stained with DAPI. Background, experiment was done without primary antibodies. Bar, 50 µm. Left panel, representative images; right panel, quantitative analysis was done using BlobFinder. Statistical analysis was done with one-way ANOVA followed by Dunnett's multiple comparison test, ** $p < 0.01$; ***$p < 0.0001$. Results were obtained from three independent experiments analyzing 60 cells per experimental condition. (C) Monolayers were cultured in LC and treated or not (vehicle only, DMSO 0.25%) for 2 h with 6 µM röttlerin. The PLA was done with a rabbit antibody against ZO-2 and a mouse antibody against pan14-3-3. Background, PLA was done in LC monolayers without both primary antibodies. Nuclei were stained with DAPI. Bar, 40 µm. Left panel, representative images; right panel, quantitative analysis done using BlobFinder. Statistical analysis was done with one-way ANOVA followed by Dunnett's multiple comparison test; ****$p < 0.0001$. Results were derived from 11 optical fields analyzed per condition from two independent experiments.

14-3-3ζ with ZO-2 in the cell borders to that in the cytoplasm. In this measure, $-1 \leq FCI < 0$ indicates that a greater extent of complexes are in the cytoplasm, while $0 < FCI \leq 1$ indicates that a greater extent of complexes is present in the cell periphery (Cruz *et al.*, 2015). In LC, ZO-2 is not present at the cell borders, hence FCC determination could not be made. Therefore, we included a SS condition that consisted of confluent monolayers incubated in NC media. Figures 6B and 7B show that in SS, FCI values are < 0 indicating that the colocalization of 14-3-3σ and 14-3-3ζ with ZO-2 was higher in the cytoplasm than in the cell borders. Instead, 2, 4, and 6 h after CS, a small but significant proportion of cells exhibited FCI > 0 indicating that in them the colocalization of 14-3-3σ and 14-3-3ζ with ZO-2 was higher at the cell borders than at the cytoplasm.

These results indicate that in the LC condition, ZO-2 is associated with 14-3-3σ and 14-3-3ζ in the cytoplasm, and that transfer to NC media induces recruitment of these complexes to the plasma membrane and their dissociation as ZO-2 incorporates into nascent TJs.

To provide a link between CaSR activation and the 14-3-3/ZO-2 complex, we next analyzed in dual-color confocal images the cytoplasmic colocalization of 14-3-3σ and 14-3-3ζ with ZO-2, after 2 h of activation of the CaSR with Gd^{3+} or of PKCε with bryostatin. Figure 8 shows in immunofluorescence images and with a subsequent PCC analysis that activation of the CaSR/PKCε signaling pathway reduces the cytoplasmic colocalization of 14-3-3 and ZO-2.

Altogether these results indicate that the activation of CaSR triggers a signaling cascade that induces the dissociation of

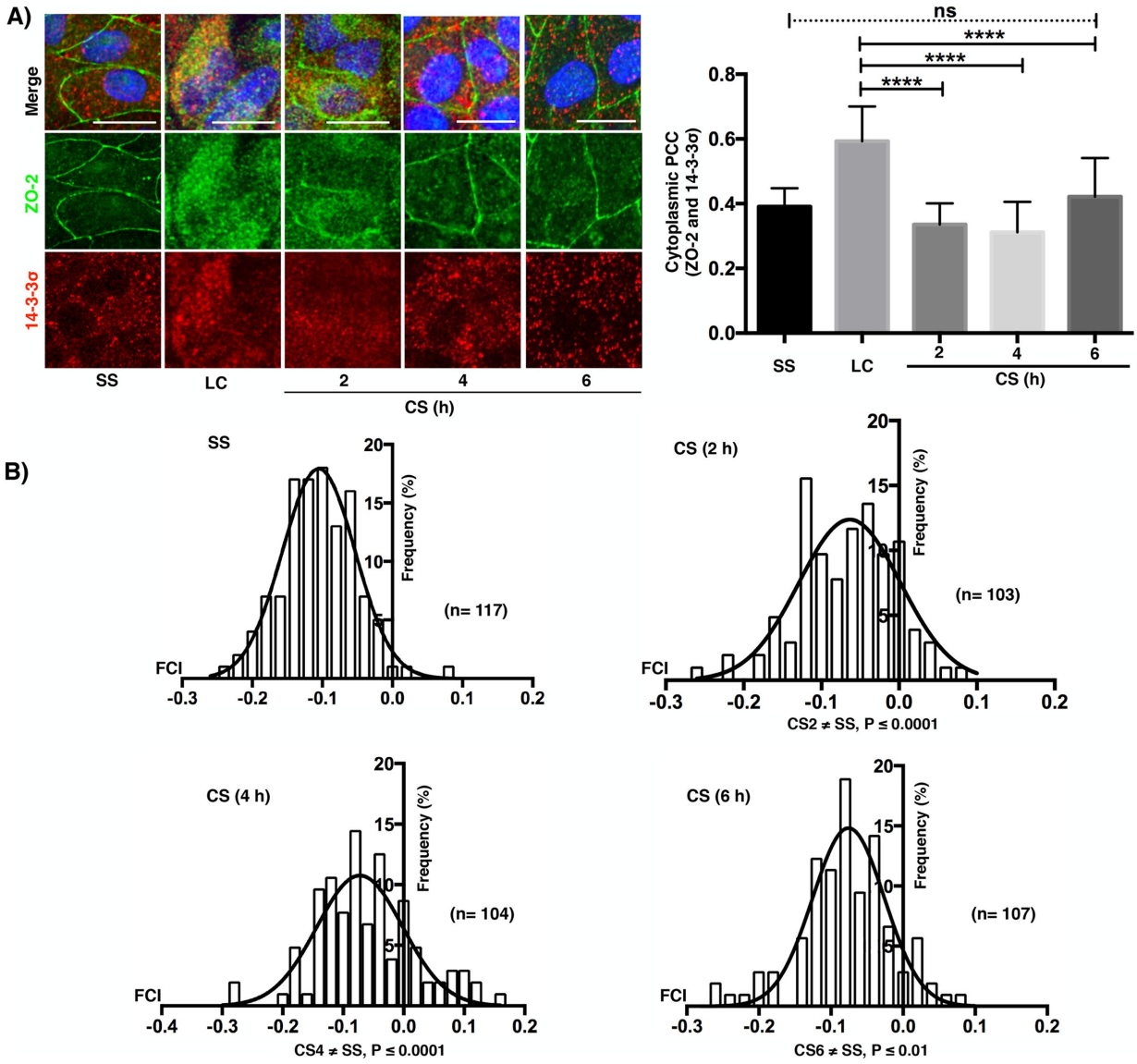

FIGURE 6: ZO-2 colocalization with 14-3-3σ in the cytoplasm of monolayers cultured in LC diminishes with the CS and is accompanied by a transient colocalization at the cell borders. (A) Immunofluorescence observation of ZO-2 and 14-3-3σ in monolayers cultured in the SS condition, LC condition for 20 h, or 2, 4, and 6 h after a CS. Left panel, representative images; right panel, cytoplasmic PCC. Statistical analysis done with Kruskal-Wallis test followed by Dunn's multiple comparison test; ****$p < 0.0001$; ns, nonsignificant. Bars, 15 μm. (B) Fluorescence covariance index (FCI = Log10 of PCC at cell periphery/PCC at cytoplasm) was done to compare the frequency of colocalization of 14-3-3σ with ZO-2 in the cell borders with the colocalization in the cytoplasm. SS, steady state condition. The values of FCI 2, 4, and 6 h after the CS are different from the SS condition since a small but significant proportion of cells exhibited FCI > 0 indicating that in them the colocalization of 14-3-3σ with ZO-2 was higher at the cell borders than at the cytoplasm. Statistical analysis done with one-way ANOVA followed by Dunnett's multiple comparison test, SS ≠ CS (2 h) ****$p < 0.0001$; SS ≠ CS (4 h) ****$p < 0.0001$; SS ≠ CS (6 h).

14-3-3/ZO-2 complexes in the cytoplasm as ZO-2 accumulates at the cell borders.

The amount of ZO-2 diminishes after CS due to lysosomal degradation

We analyzed by Western blot the cellular content of 14-3-3ζ, 14-3-3σ, and ZO-2 in LC and after CS, found that the amount of these proteins diminished with time after transfer to NC (Figure 9A). Then, we asked whether the decrease of ZO-2 was due to proteosomal or lysosomal degradation. To make sure that degradation and not new synthesis was being followed, a 5-h incubation with 30 μM cyloheximide was done in monolayers that remained in the LC condition and in those subjected to CS. Figure 9B shows that the cellular content of ZO-2 diminishes to 55% when the LC culture is treated with cycloheximide, thus revealing that even in the LC condition, where no TJ are formed, ZO-2 is being synthesized. Moreover, 5 h after CS, the decrease in the amount of ZO-2 is more pronounced when protein synthesis was inhibited with cycloheximide (18%) than when it was not (54%), thus indicating that during CS, ZO-2 is being synthesized de novo. Treatment with MG132 did not affect ZO-2 decay 5 h after CS in the absence or presence of cycloheximide. Instead, treatment with chloroquine, an agent that blocks lysosomal protein degradation by raising

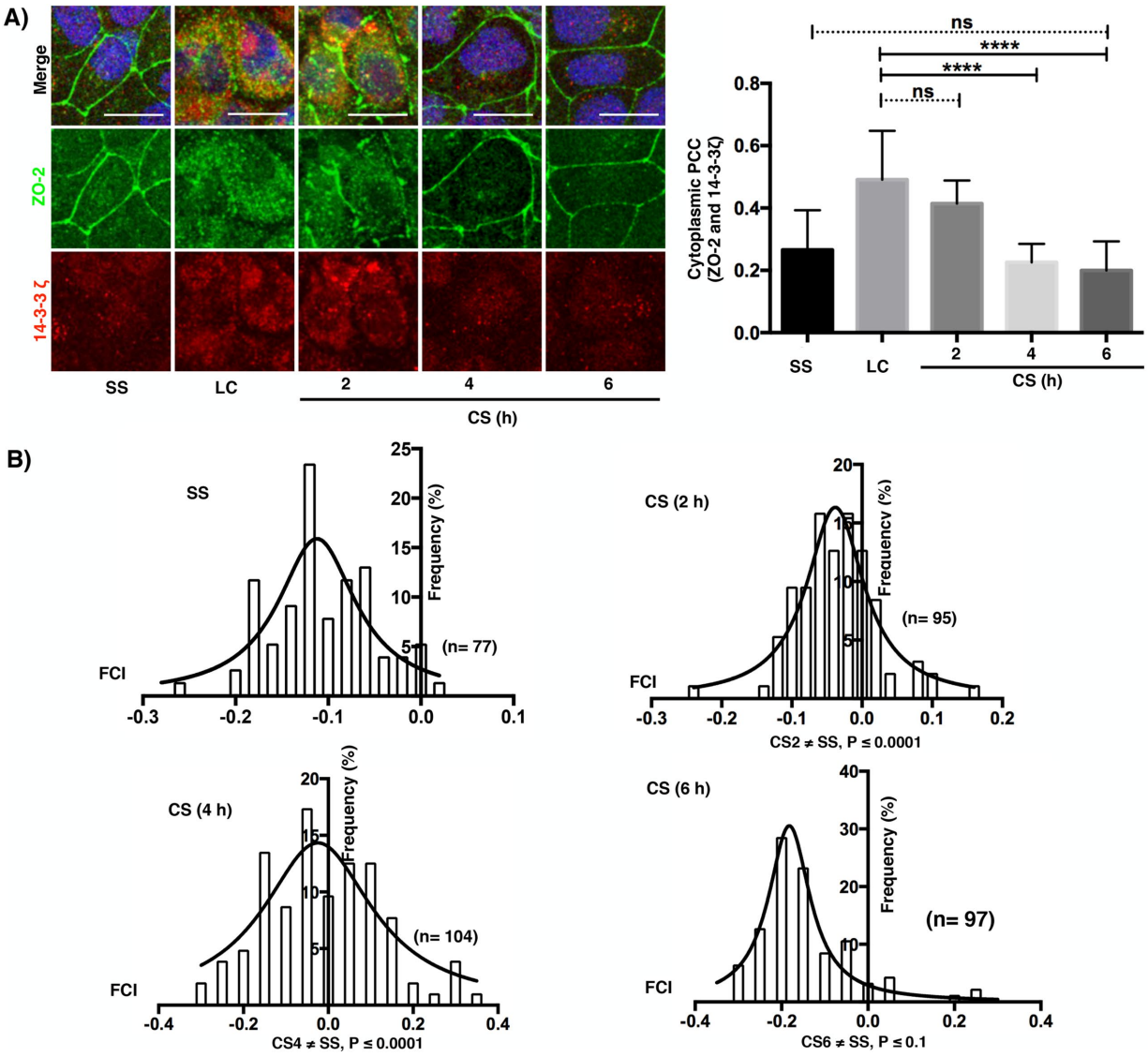

FIGURE 7: ZO-2 colocalization with 14-3-3ζ in the cytoplasm of monolayers cultured in LC diminishes with the CS and is accompanied by a transient colocalization at the cell borders. (A) Immunofluorescence observation of ZO-2 and 14-3-3ζ in monolayers cultured in the SS condition, LC condition for 20 h, or 2, 4, and 6 h after a CS. Left panel, representative images; right panel, cytoplasmic Pearson's correlation coefficient. Statistical analysis was done with Kruskal-Wallis test followed by Dunn's multiple comparison test; ****$p < 0.0001$; ns, nonsignificant. Bars 15 μm. (B) Fluorescence covariance index (FCI = Log10 PCC at cell periphery/PCC at cytoplasm) was done to compare the frequency of colocalization of 14-3-3ζ with ZO-2 in the cell borders with the colocalization in the cytoplasm. SS, steady state condition. The values of FCI 2 and 4 h after the CS are different from the SS condition since a small but significant proportion of cells exhibited FCI > 0 indicating that in them the colocalization of 14-3-3ζ with ZO-2 was higher at the cell borders than at the cytoplasm. Statistical analysis done with Kruskal-Wallis test followed by Dunn's multiple comparison test; SS ≠ CS (2 h) ****$p < 0.0001$; SS ≠ CS (4 h) ****$p < 0.0001$; SS vs. CS (6 h) nonsignificant.

lysosomal pH and inhibiting lysosomal enzymes (Rutz *et al.*, 2004) (for a review see see Steinman *et al.*, 1983), blocked ZO-2 degradation during CS when cycloheximide was added or not (Figure 9B).

Next, we analyzed the effect of chloroquine and MG132 on the degradation of 14-3-3ζ and 14-3-3σ 6 h after CS (Figure 9C), observing that their degradation is reversed by proteosomal inhibition and not by lysosomal blockade (Figure 9C).

ZO-2 is a cytoplasmic protein; hence its degradation in lysosomes instead of proteosomes, after CS, suggests that ZO-2 after reaching the plasma membrane is endocyted. To test this proposal, we incubated the monolayers during a 4-h CS with hypertonic media that inhibits receptor-mediated endocytosis (Daukas and Zigmond, 1985; Heuser and Anderson, 1989), finding that this treatment reverses the decay of ZO-2 (Figure 9D). To further confirm this observation, cells were subjected to CS in the presence or absence of dynasore, a cell-permeable GTPase inhibitor that targets dynamins –1 and –2 blocking clathrin-coated vesicle formation in endocytosis and ligand uptake through caveolae (Macia *et al.*, 2006). Figure 9E shows that dynasore blocks the decay of ZO-2 that happens after CS.

To further demonstrate the endocytosis of ZO-2, we analyzed by immunofluorescence whether after CS, ZO-2 colocalized with the early endosome marker EEA-1 (Mu *et al.*, 1995) and with Rab-7, a marker of late endosomes (for a review see Apodaca *et al.*, 2012). In

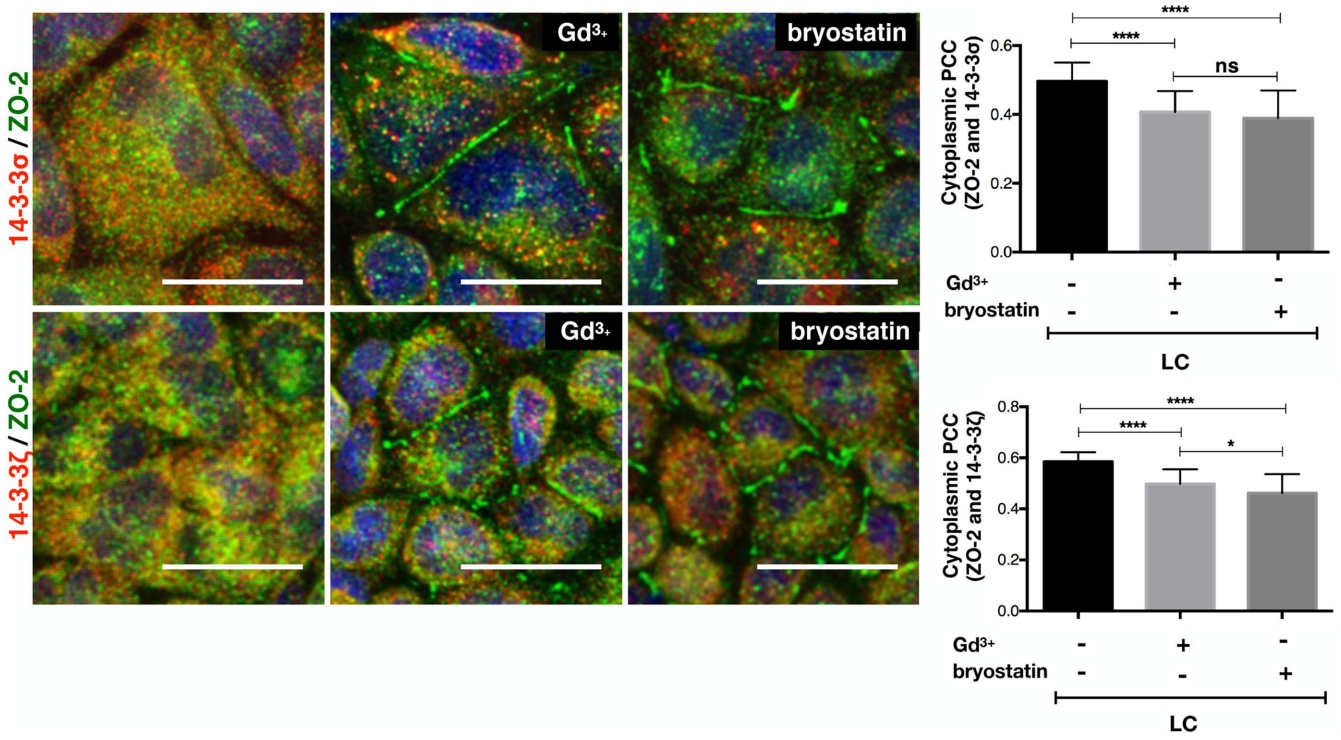

FIGURE 8: Activation of the CaSR/PKCε signaling pathway reduces the cytoplasmic colocalization of 14-3-3 and ZO-2. MDCK cells cultured in the LC condition were treated or not for 2 h with 100 μM Gd^{3+} or 200 nM bryostatin. Monolayers were processed for immunofluorescence with mouse antibodies against 14-3-3σ and 14-3-3ζ and rabbit antibodies anti-ZO-2. Left panel, representative images. Bars, 20 μm. Right panel, cytoplasmic PCC was done analyzing 100 cells per condition derived from two independent experiments. Statistical analysis done with Kruskal-Wallis followed by Dunn's multiple comparison test; $^{****}p < 0.0001$; $^{*}p < 0.01$.

this experiment, the monolayers were incubated with 50 μM chloroquine to block the degradation of ZO-2 in the lysosome. Figure 10 shows that ZO-2 can be found colocalizing with EEA-1 120 min after the CS, whereas the colocalization with Rab-7 is evident 240 min after the CS. These results thus indicate that after the CS, ZO-2 is endocyted.

Taken together, these results indicate that ZO-2 is degraded in the cytoplasm in the LC condition; however, a certain amount of ZO-2 is protected from degradation due to its association to 14-3-3 in the cytoplasm. After CS, ZO-2/14-3-3 complexes relocalize to the cell borders and dissociate. The 14-3-3 is then degraded in the proteosome, while ZO-2 associates to the TJs that are being assembled de novo (Gonzalez-Mariscal *et al.*, 1985). There the number of ZO-2 binding sites might be limited (Chamorro *et al.*, 2009), inducing the endocytosis and degradation of excessive ZO-2 in the lysosome.

The unique region 2 (U2) of ZO-2 is critical for the interaction of the molecule with 14-3-3

With regard to 14-3-3 putative binding sites on ZO-2, Supplemental Table 1 and Figure 4A show that hZO-2 has 10 sites for a total of 22 located in the U2 region, while cZO-2 has 11 sites for a total of 25 in this region. This observation is particularly relevant, since 14-3-3 binding motifs are very frequently located within disordered regions that border functional domains (Bustos and Iglesias, 2006; Oldfield *et al.*, 2008; Johnson *et al.*, 2010; Uhart and Bustos, 2014), and the ZO-2 U2 segment that localizes between PDZ1 and PDZ2 domains has no inherent structure according to JPred protein secondary structure prediction system (www.compbio.dundee.ac.uk/jpred/). This condition might give a greater capture radius of ligands to the U2 segment than a compact folded region and in addition suggests that binding to 14-3-3 could induce a disorder to order transition of ZO-2 as has been suggested for other proteins that bind to 14-3-3 (Bustos and Iglesias, 2006).

To test the importance of the U2 segment, we next transfected MDCK cells with a wild-type (WT) hZO-2 (Flag-hZO-2) construct or a hZO-2 construct lacking the U2 region (Flag-hZO-2 ΔU2) and analyzed the in situ interaction between ZO-2 and 14-3-3, with a PLA employing a rabbit antibody against Flag and mouse antibodies against 14-3-3σ and 14-3-3ζ. We observed in the transfected cells cultured in LC that the positive red fluorescent spots that reveal the interaction between Flag-hZO-2 and 14-3-3σ (Figure 11A, top panel) or 14-3-3ζ (Figure 11A, bottom panel) diminish when ZO-2 lacks the U2 segment. To further confirm these results, in MDCK cells cultured in LC and transfected with Flag-hZO-2 or Flag-hZO-2 ΔU2, we made an immunoprecipitation assay with an antibody against Flag. The Western blot revealed that the lack of the U2 segment in ZO-2 diminished the coimmunoprecipitation of 14-3-3σ and 14-3-3ζ (Figure 11B). These results thus indicate that the U2 region of ZO-2 is critical for the interaction of the molecule with 14-3-3.

S261 is crucial for cZO-2 binding to 14-3-3σ and 14-3-3ζ and importation into the nucleus

We observed that seven of the 11 putative 14-3-3 binding sites present within the U2 region of cZO-2 form part of SR repeats (Figure 4A and Supplemental Table 1), which on phosphorylation by the enzyme SRPK induce the accumulation of ZO-2 at nuclear speckles (Quiros *et al.*, 2013). In addition, cZO-2 residues Thr248 and Ser261 are located within bipartite nuclear localization signal 2 (bpNLS-2) (Figure 4A and Supplemental Table 1) Since it had been previously shown that the association of 14-3-3 with a nuclear localization

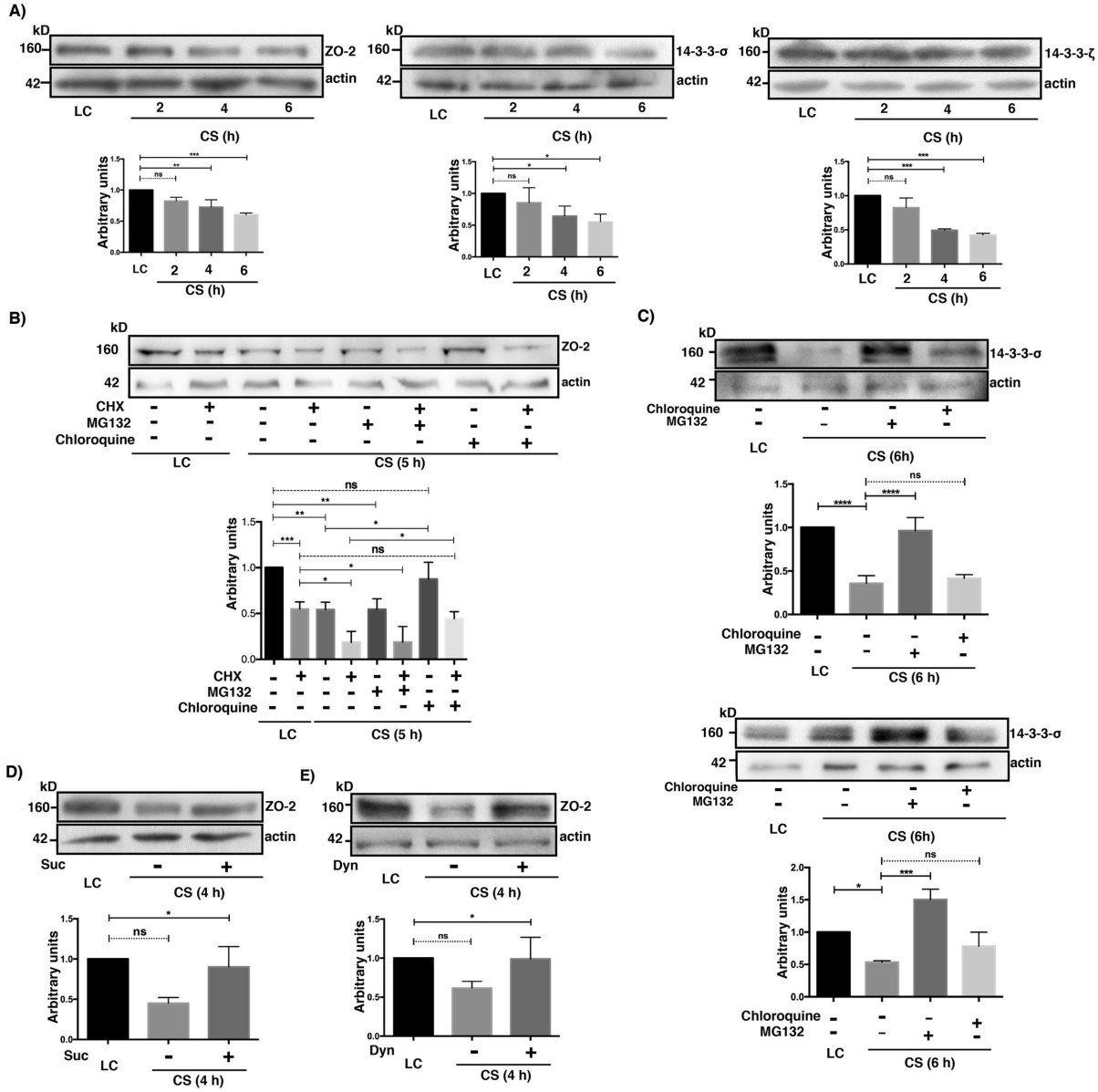

FIGURE 9: The cellular content of ZO-2 diminishes after the CS due to lysosome-mediated degradation. (A) The amount of ZO-2, 14-3-3σ, and 14-3-3ζ diminishes with the CS. Cell lysates were obtained from monolayers cultured in the LC condition for 20 h or 2, 4, and 6 h after a CS. Top panels, representative Western blots; bottom panels, densitometric analysis. Statistical analysis done with One Way ANOVA followed by Dunnett's multiple comparison test. ns, not significant; *$p < 0.05$; **$p < 0.01$; ***$p < 0.001$. All the results in this figure correspond to at least three independent experiments. (B) The decay of ZO-2 triggered by the CS can be reversed with cloroquine but not with MG132. Cell lysates were obtained from monolayers cultured in the LC condition for 20 h and incubated or not for 5 additional h with 30 μM cycloheximide (CHX) or transferred to NC media (CS) for 5 h in the presence or absence of 30 μM cycloheximide (CHX) with or without 30 μM MG132 or 50 μM cloroquine. Top panel, representative Western blot; bottom panel, densitometric analysis. Statistical analysis done with one way ANOVA followed by Dunnett's multiple comparison test; ns, not significant; ***$p < 0.001$; **$p < 0.01$; *$p < 0.05$. (C) The 14-3-3σ and 14-3-3ζ are degraded in the proteosome and not in the lysosome during the CS. Cell lysates were obtained from monolayers cultured in the LC condition for 20 h or transferred to NC media (CS) for 6 h in the presence or absence of 30 μM MG132 or 50 μM cloroquine. Top panel, representative Western blot; bottom panel, densitometric analysis. Statistical analysis done with one way ANOVA followed by Dunnett's multiple comparison test. ns, not significant; *$p < 0.05$; ***$p < 0.001$. (D) The decrease in ZO-2 content is mediated by receptor-mediated endocytosis. Cell lysates were obtained from monolayers cultured in the LC condition for 20 h or transferred to NC media (CS) for 4 h in the presence or absence of 0.45 M sucrose (Suc). Top panel, representative Western blot; bottom panel, densitometric analysis. Statistical analysis done with one way ANOVA followed by Dunnett's multiple comparison test; ns, not significant; *$p < 0.05$. (E) The decay of ZO-2 present after the CS is due to dynamin-dependent endocytosis. Cell lysates were obtained from monolayers cultured in the LC condition for 20 h or subjected to a CS for 4 h in the presence or absence of 80 μM dynasore. Top panel, representative Western blot; bottom panel, densitometric analysis. Statistical analysis done with one way ANOVA followed by Dunnett's multiple comparison test; ns, not significant; *$p < 0.05$.

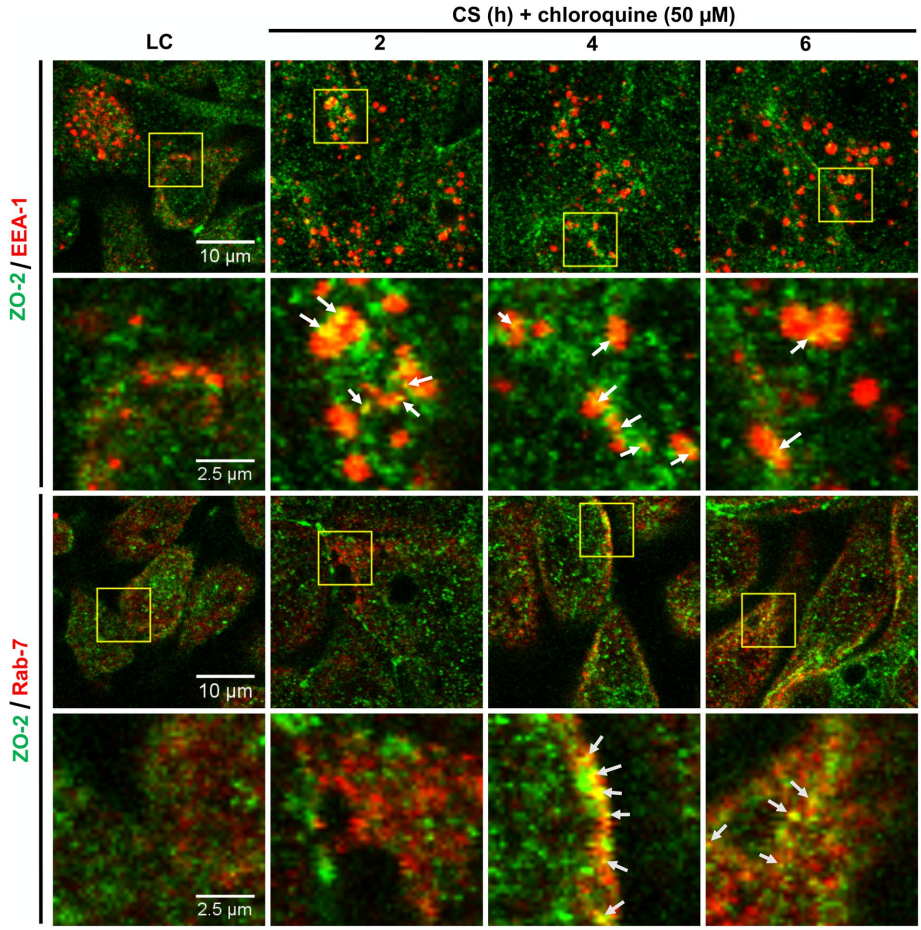

FIGURE 10: ZO-2 is endocyted and reaches late endosomes during the CS. Monolayers incubated in the LC condition or transferred to NC media for different periods of time were processed for immunofluorescence with antibodies against ZO-2, the early endosomal marker EEA-1 and the late endosomal marker Rab7. Representative images are from three independent experiments.

signal present in FOXO1 blocked the nuclear importation of this transcription factor (Zhao *et al.*, 2004), we next tested whether HA-cZO-2 mutants T248A and S261A altered the nuclear importation of the protein. Figure 12A shows, as we previously reported (Chamorro *et al.*, 2009; Quiros *et al.*, 2013), that in NC medium, 80% of cells transfected with WT HA-cZO-2 express ZO-2 protein at the nucleus at time 0, which corresponds to 6 h after transfection, a time needed after transfection, for proteins to be expressed. The percentage of cells with nuclear WT HA-cZO-2 diminishes with time as the monolayer becomes confluent, as we previously observed (Chamorro *et al.*, 2009; Quiros *et al.*, 2013). Instead, only 16% of the cells expressing HA-cZO-2 mutant S261A have it at the nucleus at time 0, while mutant T248A exhibits only a slightly delayed nuclear recruitment (62% at time 0). To further confirm that S261 is crucial for cZO-2 nuclear importation, we made a Western blot of a cell fractionation assay (Figure 12B). The quantitative analysis of the nuclear, membrane, and cytoplasm fractions showed that while 46.4% of WT HA-cZO-2 was present at the nucleus at time 0, only 0.2% was detected 24 h later, whereas a barely detectable amount of the HA-cZO-2 mutant S261A was present in the nucleus both at time 0 and 24 h later. The amount of HA-cZO-2 mutant S261A found in every fraction is lower than that of HA-cZO-2 and the mutant S261A concentrates in the membrane fraction since time 0 (Figure 12B). To demonstrate the presence of HA-cZO-2 mutant S261A in all the cellular fractions, albeit at low intensity, a high exposure blot is also shown (Figure 12A, right panel)

Taken together, these results indicate that S261 present within the bpNLS-2 is crucial for an efficient importation of ZO-2 into the nucleus and suggest that the decreased cellular content of HA-cZO-2 mutant S261A might be due to its decreased capacity to associate to 14-3-3 that may render it more susceptible to proteosomal degradation. To further explore this point, we analyzed by Western blot the total cellular content of HA-cZO-2 and the mutants T248A and S261A in LC-cultured cells in the presence or absence of MG132. Figure 12C reveals that the expression of both HA-cZO-2 mutants recovers to control values after treatment with MG132, thus indicating that their reduced expression is due to proteosomal degradation.

Next, we analyzed by immunofluorescence whether newly synthesized cZO-2-HA colocalized with 14-3-3 σ and ζ in the nucleus, observing that their initial nuclear colocalization at time 0 (6 h after transfection) diminished 24 h later (Figure 12D, top panel) when the percentage of cells with nuclear ZO-2 is significantly reduced (Figure 12A). With PCC we confirmed these observations (Figure 12D, bottom panel).

Since residues T248 and S261 are putative 14-3-3 binding sites, we next tested with a PLA the interaction between HA-cZO-2 mutants lacking these residues and endogenous 14-3-3σ or ζ. For this purpose, cells were transfected with WT HA-cZO-2 or the HA-cZO-2 mutants T248A and S261A. The PLA was done in the presence of MG132 to avoid proteosomal degradation of HA-cZO-2 mutants, with a rabbit antibody against HA and a mouse antibody against 14-3-3σ or ζ. Figure 13, A and B, shows that the interaction between 14-3-3 σ or ζ and ZO-2 mutants T248A and S261A decreases in comparison to that with WT HA-cZO-2, with the decrease more pronounced for the ZO-2 S261A mutant. To further reinforce these results, an immunoprecipitation assay was done, confirming a decreased interaction only between 14-3-3 and ZO-2 mutant S261A (Figure 13C).

Taken together, these results suggest that S261 located within bpNLS-2 is a binding site for 14-3-3σ and ζ, and that this interaction facilitates the importation of ZO-2 into the nucleus.

DISCUSSION

ZO-2 is a protein that shuttles among the cytoplasm, the nucleus, and TJs. In sparse epithelial cells, the movement of newly synthesized ZO-2 into the nucleus is regulated by NLSs and phosphorylation of serine/arginine (SR) repeats (Quiros *et al.*, 2013), while nuclear exportation of ZO-2 occurs when cells become confluent in a process mediated by nuclear exportation signals (NESs) (Jaramillo *et al.*, 2004; Gonzalez-Mariscal *et al.*, 2006), the phosphorylation-dependent activation of a NES (Chamorro *et al.*, 2009) and the inactivation of a NLS by SUMOylation (Wetzel *et al.*, 2017). In confluent

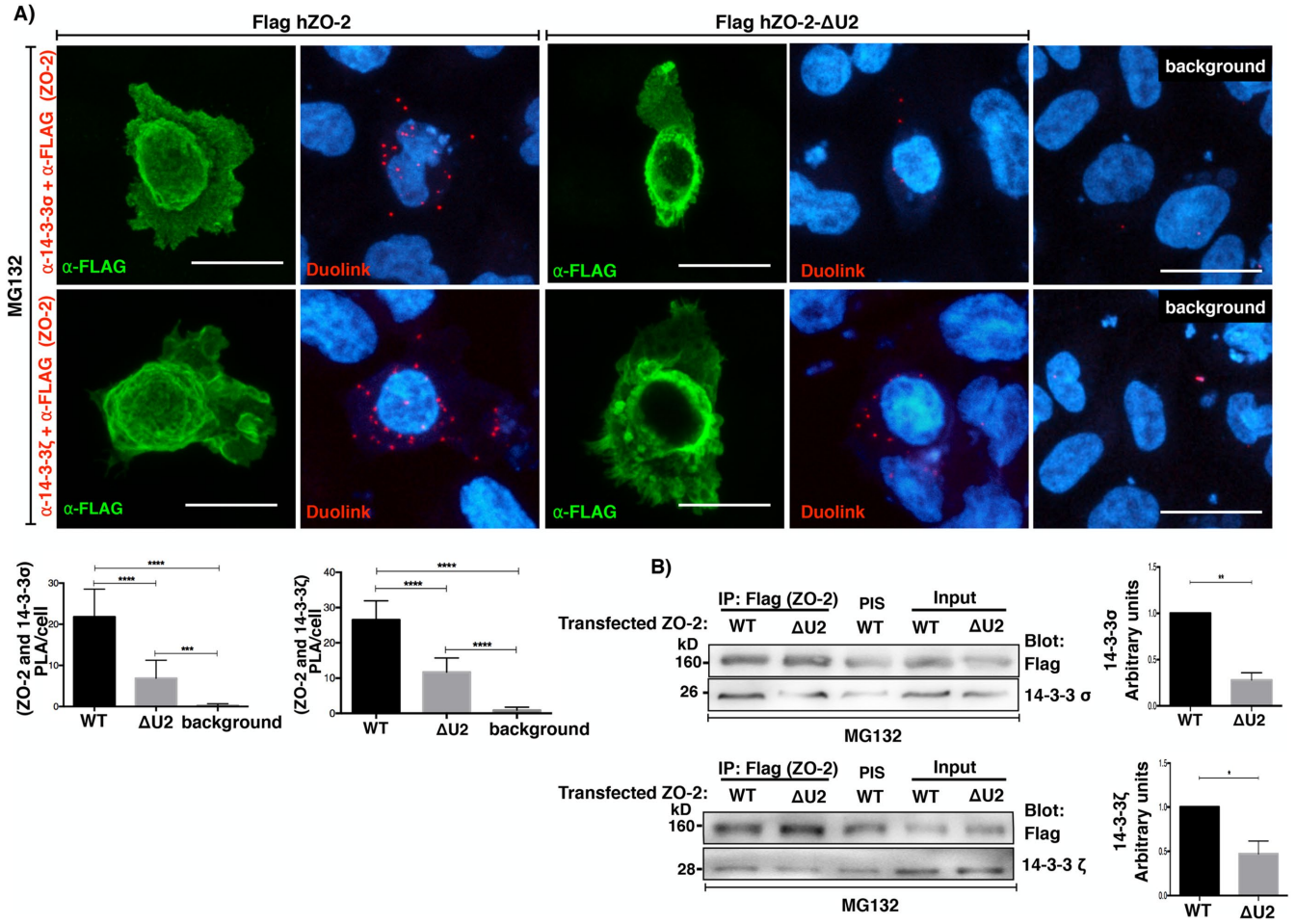

FIGURE 11: The U2 segment of ZO-2 favors the interaction of ZO-2 with 14-3-3. MDCK monolayers cultured in LC medium were transfected with WT hZO-2 (Flag-hZO-2) or a hZO-2 lacking the U2 region (Flag-hZO-2 ΔU2) and treated with 30 μM MG132 for 4 h. (A) A PLA assay was done employing a rabbit antibody against Flag and mouse antibodies against 14-3-3σ or 14-3-3ζ. Transfected cells were identified by their green staining after treatment with an antibody against rabbit coupled to Alexa Fluor 488. Background, untransfected cells. Bars, 15 μm. Top panel, representative images; bottom panel, quantitative analysis was done using BlobFinder. Statistical analysis done with one-way ANOVA followed by Dunnett's multiple comparison test; ***$p < 0.001$; ****$p < 0.0001$. Results were obtained analyzing 20 transfected cells per condition derived from two independent experiments. (B) Immunoprecipitation assay was done with an antibody against Flag and blotted with antibodies against Flag, 14-3-3σ, and 14-3-3ζ. PIS, preimmune serum. Left panels, representative images; right panels, quantitative analysis of three independent experiments. Statistical analysis done with student's *t* test; *$p < 0.05$; **$p < 0.01$.

cultures instead, newly synthesized ZO-2 reaches the TJ without making a stopover at the nucleus (Quiros *et al.*, 2013).

In this work, we sought to unveil the molecular mechanism that induces the translocation of ZO-2 from the cytoplasm to the TJs. We have employed a model of epithelial MDCK cells cultured in LC, since in this system we had previously observed that ZO-2 is diffusely distributed in the cytoplasm and because with Gd^{3+}, we could test whether the relocation of ZO-2 to the plasma membrane started by activation in the membrane of the CaSR. Our observation that Gd^{3+} triggers the appearance of discontinuous stretches of ZO-2 at the borders of cells cultured in LC media is consistent with previous reports showing that CaSR agonists neomycin, Gd^{3+}, and R-568 cause the recruitment of ZO-1 and occludin to sites of cell–cell contact in cells cultured in LC (Jouret *et al.*, 2013). The importance of CaSR for TJ regulation is further reinforced by the observation that this receptor accelerates the expression profile of claudins during epidermal differentiation (Troy *et al.*, 2007) and promotes the expression of claudin-14 in the kidney (Toka *et al.*, 2012) through the down-regulation of specific microRNAs (Gong *et al.*, 2012).

Surprisingly, we found that in the LC condition the amount of ZO-2 detected in the membrane fraction by Western blot does not augment after inhibition of 14-3-3 with BV02, suggesting that the discontinuous stretches of ZO-2 observed by immunofluorescence at the cell borders of LC-cultured cells after activation of the Gd^{3+}/CasR/PKCε/WNK4 pathway might correspond to polymerized ZO-2 that due to its previous association to 14-3-3 was undetectable by immunofluorescence in the plasma membrane.

Since DiC8, a permeable DAG, induces the appearance of ZO-2 at the border of cells cultured in LC, we conclude that a cPKC or nPKc was involved. Previously we had shown that treatment with DiC8 triggered the appearance of ZO-1 at cell borders in cells cultured in LC (Balda *et al.*, 1993) and that nPKCε induces the exit of ZO-2 from the nucleus (Chamorro *et al.*, 2009). Moreover, treatment with the traditional Chinese medicine, indigo naturalis (Lin *et al.*, 2013), or the anti-inflammatory molecule, oxyresveratrol

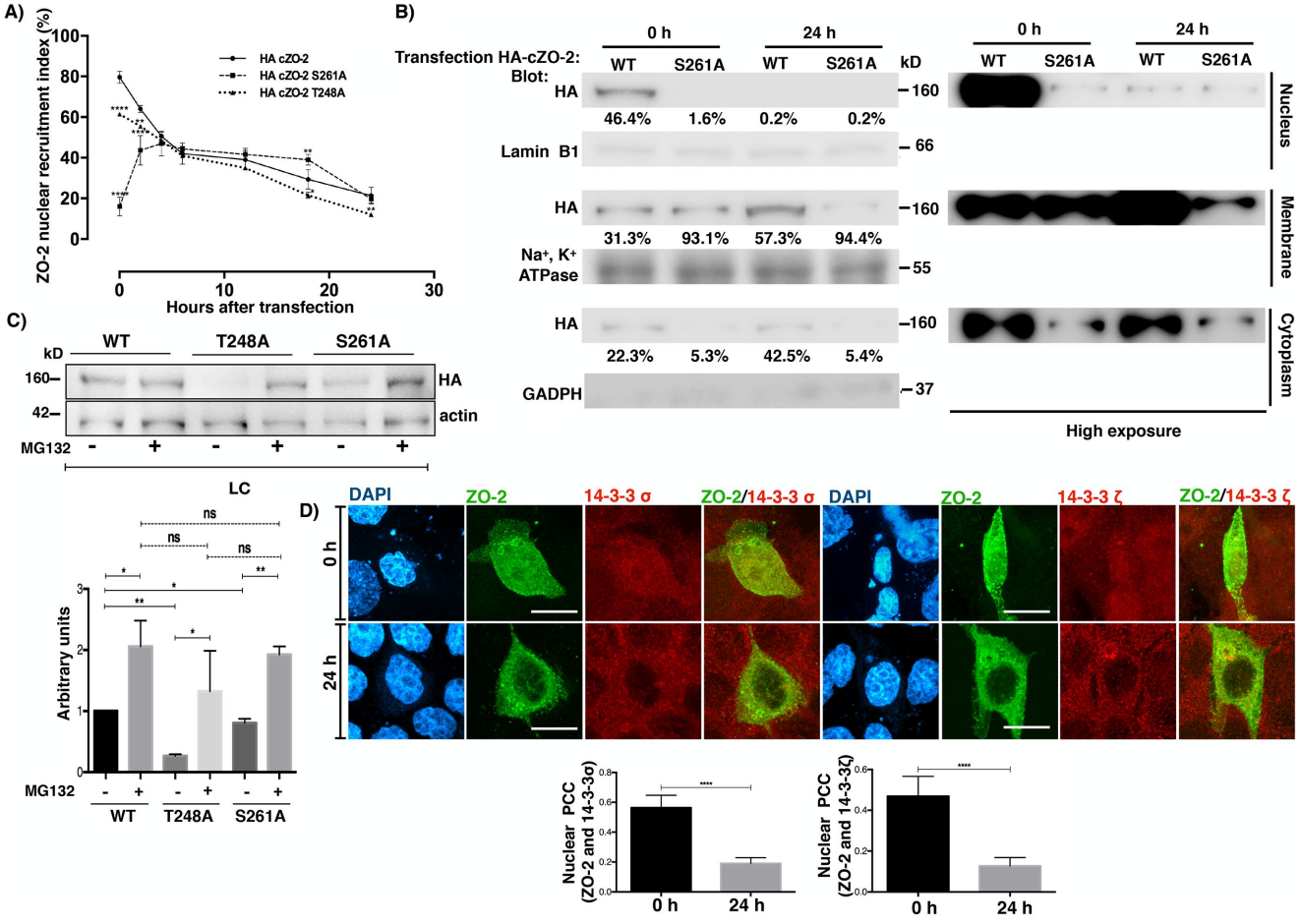

FIGURE 12: ZO-2 colocalizes with 14-3-3 in the nucleus, and residue S261 of cZO-2 is crucial for the nuclear importation the protein. (A) Left panel, percentage of cells with nuclear HA-ZO-2 as a function of time after transfection, determined by immunofluorescence using an anti HA antibody. Monolayers cultured in NC media were fixed at the indicated times. Time 0 corresponds to 6 h after transfection. Experiments were done with cells transfected with HA-cZO-2 WT, HA-cZO-2 S261A, and HA-cZO-2 T248A. Results are from three independent experiments. In each experiment, 100 transfected cells were evaluated per experimental point. Statistical analysis done with two way ANOVA followed by Bonferroni's multiple comparison test. cZO-2 S261A and HA-cZO-2 T248A were compared against HA-cZO-2 WT; *$p <$ 0.05; **$p < 0.01$; ***$p < 0.001$; ****$p < 0.0001$. (B) Western blot against HA-ZO-2 present in nuclear, cytoplasmic, and plasma membrane fractions of cells at times 0 and 24 h of transfection with HA-cZO-2 WT and HA-cZO-2 S261A. Antibodies against lamin B1, Na^+,K^+-ATPase β1 subunit, and GAPDH were employed as markers of nuclear, plasma membrane, and cytoplasmic fractions, respectively. Right panel, overexposed Western blot. (C) The reduced cellular content of HA-cZO-2 mutants T248A and S261A in comparison to WT HA-cZO-2 in LC cultured cells, recovers after proteasome inhibition with MG132. Western blot of cellular lysates derived from monolayers transfected with WT HA-cZO-2 or the mutants T248A and S261A in the presence or absence of 30 μM MG132. Statistical analysis was done with one-way ANOVA followed by Dunnett's multiple comparisons test, *$p < 0.05$; **$p < 0.01$. Results were obtained from three independent experiments. (D) cZO-2-HA colocalized with 14-3-3 σ and ζ in the nucleus at time 0 (6 h after transfection) and this interaction diminished 24 h later. Monolayers were transfected with HA-cZO-2 WT. Immunofluorescence done with antibodies against 14-3-3σ or 14-3-3ζ and anti HA. Top panel, representative images; bottom panel, PCC in the nucleus. Bars, 20 μm. Statistical analysis was done with two-tailed Student's *t* test, ****$p <$ 0.0001. Results were obtained from 20 transfected cells per experimental condition from to independent experiments.

(Jo *et al.*, 2017), increased TJ function and protein expression through a process mediated by PKC activation. In a similar manner, treatment of intestinal cells with probiotic secretory proteins (Seth *et al.*, 2008), or bile duct epithelia with EGF (Guntaka *et al.*, 2011), protected TJ barrier function from hydrogen peroxide-induced insult through a mechanism mediated by cPKC and nPKCε. PMA, a phorbol ester that activates cPKC and nPKC, increased TER in intestinal HT-29 cells (Sjo *et al.*, 2003), while the stimulation of Toll-like receptor 2 increased TER and concentrated ZO-1 at the TJ through a process mediated by the activation of cPKCα and nPKCδ (Cario *et al.*, 2004). Bryostatin, a specific activator of cPKCα and nPKC δ and ε, restored blood–brain barrier (BBB) integrity and increased the expression of ZO-1 following blast-induced traumatic brain injury (Lucke-Wold *et al.*, 2015); in T84 cells bryostatin induced the subcellular redistribution of ZO-2 from a detergent-soluble fraction to a detergent-insoluble fraction. This process appeared to be mediated by nPKCε, as it was not inhibited by the cPKC inhibitor Gö-6976 or the PKCδ-specific inhibitor röttlerin, but only by the inhibitor of conventional and novel PKCs Gö-6850 (Yoo *et al.*, 2003). Röttlerin instead exacerbated BBB hyperpermeability and TJ

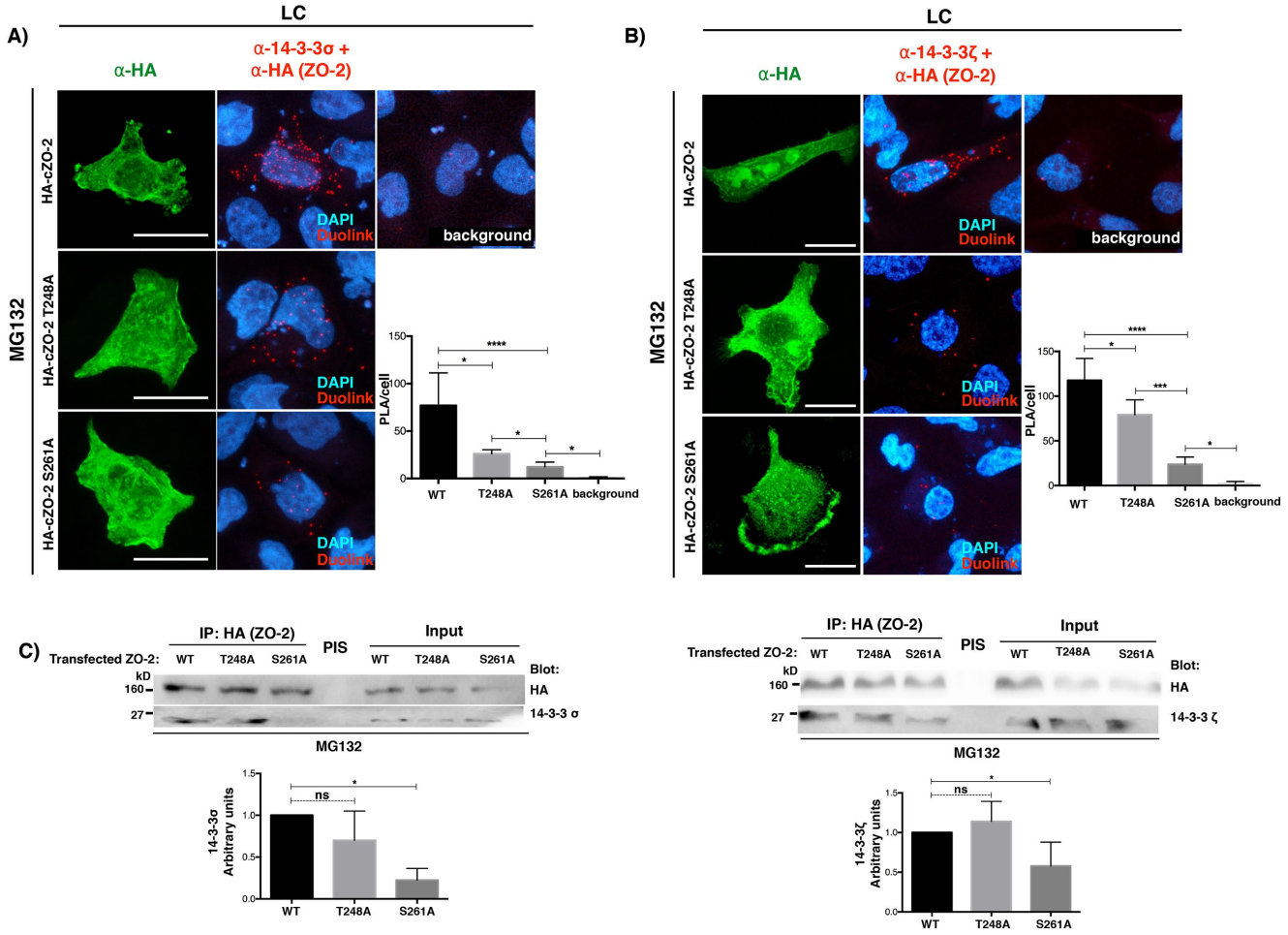

FIGURE 13: cZO-2 mutants S261A and T248A displays reduced binding to 14-3-3σ and 14-3-3ζ. (A) The interaction of endogenous 14-3-3σ and transfected HA-cZO-2 diminishes with cZO-2 mutants S261A and T248A. Cells were transfected with WT HA-cZO-2 or the HA-cZO-2 mutants T248A and S261A. PLA was done with a rabbit antibody against HA and a mouse antibody against 14-3-3σ in the presence of MG132. In this experiment, the cells transfected with HA-cZO-2 or the HA-cZO-2 mutants T248A and S261A were identified with a rabbit antibody against HA, followed by a secondary anti rabbit antibody coupled to Alexa Fluor 488. Background corresponds to cells not transfected with HA-cZO-2. Bars, 15 μm. Left panel, representative images; right panel, quantitative analysis done using BlobFinder. Statistical analysis was done with Kruskal-Wallis test followed by Dunn's multiple comparison test; *$p < 0.05$; ****$p < 0.0001$. Results were obtained with 30 transfected cells per condition derived from two independent experiments. (B) The interaction of endogenous 14-3-3ζ with transfected HA-cZO-2 diminished in mutants cZO-2 S261A and T248A. Cells were transfected with HA-cZO-2 or the HA-cZO-2 mutants T248A and S261A. PLA were done in the presence of MG132 with a rabbit antibody against HA and a mouse antibody against 14-3-3ζ. In this experiment, the transfected cells were identified with a rabbit antibody against HA, followed by a secondary anti rabbit antibody coupled to Alexa Fluor 488. Background corresponds to cells not transfected with HA-cZO-2. Bars, 20 μm. Results were obtained from 30 transfected cells per condition derived from two independent experiments. Left panel, representative images; right panel quantitative analysis done using BlobFinder. Statistical analysis done with Kruskal-Wallis test followed by Dunn's multiple comparison test; *$p < 0.05$; ***$p < 0.001$; ****$p < 0.0001$. (C) The interaction between cZO-2 and 14-3-3σ or 14-3-3ζ diminishes in the mutant HA-cZO-2 S261A but not in the mutant HA-cZO-2 T248A. Cells cultured in LC condition were transfected with WT HA-cZO-2 or the HA-cZO-2 mutants T248A and S261A. ZO-2 was immunoprecipitated with a mouse antibody against HA and blotted with a mouse antibody against 14-3-3σ or a rabbit antibody against 14-3-3ζ. Left panel, representative image of 14-3-3σ blot; right panel, representative image of 14-3-3ζ blot. Bottom panels, quantitative analysis done with one-way ANOVA; *$p < 0.05$.

disruption during aglycemic hypoxia, suggesting a protective role of PKCδ in the maintenance of the BBB (Kim *et al.*, 2010). Similarly, in the preimplantation mouse embryo, activation of nPKCδ accelerated the early assembly of ZO-2 (Eckert *et al.*, 2004). In agreement, here we observed that treatment with bryostatin, at a dose that specifically activates nPKC δ and ε, decreases the cytoplasmic colocalization of the 14-3-3/ZO-2 complex and triggers the appearance of ZO-2 at the borders of cells cultured in LC, and that röttlerin failed to inhibit this process, suggesting that nPKCδ is not required and that activation of nPKCε is sufficient to induce ZO-2 appearance at TJs triggered by CaSR activation or alternatively that either nPKCε or δ can drive this process. However, when we stimulated

LC-cultured cells with DiC8 or bryostatin and in addition employed Ro-318220 that inhibits nPKCε but not nPKCδ, or nPKCε-specific inhibitor peptide εν1-2, we observed that ZO-2/WNK4 interaction diminishes, thus indicating that nPKCε and not nPKCδ, is required for ZO-2 appearance at the cell borders.

cZO-2 is a phosphorylation target of PKC (Avila-Flores *et al.*, 2001) and contains 26 putative high stringency PKC phosphorylation sites (program GPS-3.0; Xue *et al.*, 2008); therefore, it was not surprising to find that PKC activation with DiC8 induced the serine phosphorylation of ZO-2 at PKC phosphorylation consensus sites.

We explored whether the signaling cascade triggered by CaSR that translocates ZO-2 to TJs, involved the activation of WNK4, because this kinase localizes at TJs in the distal nephron (Wilson *et al.*, 2001) and binds and phosphorylates claudins –1 to –4 (Yamauchi *et al.*, 2004). In addition, WNK proteins are essential for ion homeostasis in the nervous system and kidney (for reviews see Rodan and Jenny, 2017, and Shekarabi *et al.*, 2017). Moreover, CaSR activation induces through PKC the phosphorylation and activation of WNK4 (Bazua-Valenti *et al.*, 2018) as well as the phosphorylation and inactivation of Kelch-like 3 (Shibata *et al.*, 2014), a component of the E3-RING ubiquitin ligase complex that targets WNK4 for ubiquitination and degradation (Shibata *et al.*, 2013). This allows the CaSR to regulate NaCl reabsorption in the distal convoluted tubule by increasing the activity of the thiazide-sensitive NaCl cotransporter through the WNK4-SPAK pathway (Bazua-Valenti *et al.*, 2018).

Here, we observed that PKC stimulation induces ZO-2 interaction with WNK4, ZO-2 phosphorylation in serine residues and its relocation to the cell borders, and that these effects are blocked by inhibition of WNK proteins, indicating that farther downstream in the CaSR/PKC signaling cascade, WNK4 is involved. ZO-2 contains six high stringency putative WNK4 phosphorylation sites distributed in different segments of the molecule (Supplemental Table 2). We do not know how the phosphorylation of any or some of these residues by WNK4 triggers ZO-2 disassembly from 14-3-3 and its incorporation into TJs. However, we observed that none of the 14-3-3 putative binding sites in ZO-2 are also putative WNK4 phosphorylation sites. Therefore we think that a dual phosphorylation switch might regulate the appearance of ZO-2 at the cell borders. The first, triggered by a serine/threonine kinase different from WNK4 that allows the association of ZO-2 to 14-3-3, the subsequent maintenance of ZO-2 in a nonpolymerized state in the membrane, and the cytoplasm of cells cultured in LC. This kinase could be nPKCδ since treatment with röttlerin inhibits the interaction of ZO-2 with 14-3-3 in the cytoplasm of cells cultured in LC. The second phosphorylation is due to WNK4 that reduces the affinity of ZO-2 for 14-3-3 proteins and facilitates the polymerization and incorporation of ZO-2 into nascent TJs. In this respect, such a situation has been observed in the two-pore domain K channel TASK-1, where the phosphorylation of S393 creates a high-affinity 14-3-3 binding site that overlaps a COPI vesicle-binding motif allowing the protein to leave the early secretory pathway and to reach the cell surface, while phosphorylation of S392 reduces the affinity of 14-3-3 proteins for TASK-1, keeping the channel at the Golgi (Kilisch *et al.*, 2016).

Another case in which the localization of a TJ protein is regulated by interaction with 14-3-3 is that of ubinuclein. The latter is a ubiquitously expressed nuclear protein that in confluent monolayers concentrates at TJs interacting with ZO-1 and cingulin (Lupo *et al.*, 2012). Ubinuclein localization at TJs and especially at tricellular intersections increases on association to 14-3-3 and disappears when PKA-mediated phosphorylation of ubinuclein is inhibited (Conti *et al.*, 2013).

Interaction with 14-3-3 also regulates the nucleo-cytoplasmic shuttling of ZO-2, as the mutation in ZO-2 of 14-3-3 binding site S261 located within a NLS impairs the nuclear importation of the protein. In a similar manner, the interaction with 14-3-3 promotes the nuclear importation of yeast phosphatidylinositol 4-kinase, Pik1p (Demmel *et al.*, 2008). In contrast, the association of 14-3-3 with residues located within a NLS of FOXO1 blocks the nuclear importation of this transcription factor (Zhao *et al.*, 2004).

The association to 14-3-3 also promotes the nuclear exportation of transcription factor FKHRL1 (Brunet *et al.*, 2002), the phosphatase and mitotic inducer Cdc25 (Kumagai and Dunphy, 1999), and the chaperone Chibby in interaction with β-catenin (Li *et al.*, 2008). Instead, the association of 14-3-3 with the telomerase catalytic subunit TERT blocks the recognition of its NES by exportin CRM1, inhibiting the nuclear exportation of the telomerase (Seimiya *et al.*, 2000).

The appearance of ZO-2 at the cell border triggered by the activation of AMPK by AICAR is not surprising since previously a similar situation had been observed for ZO-1 (Zhang *et al.*, 2006). Moreover, AMPK is phosphorylated and activated by liver kinase-β1 (Zheng and Cantley, 2007), a kinase that induces cell-autonomous polarization in intestinal epithelial cells (Baas *et al.*, 2004), and by Ca^{2+}-calmodulin–dependent protein kinase kinase (Rowart *et al.*, 2017), and both proteins modulate the assembly of TJs in epithelial cells. However, this stimulation of TJ assembly appears to be independent to that triggered by the activation of CaSR, since even though PKC can stimulate adenylylcyclase leading to the activation of AMPK, the appearance of ZO-2 at the cell border is not blocked when DiC8-treated cells are incubated with the AMPK inhibitor dorsomorphin.

We observed that the amount of ZO-2 diminishes after CS, because the protein is endocyted from the plasma membrane and degraded in lysosomes. This observation was expected because previously we had demonstrated that the amount of newly synthesized endogenous ZO-2 that incorporates in the plasma membrane is limited, in contrast to that which accumulates in the nucleus that seems to serve as a cellular reservoir of ZO-2, subject to drastic amount variations (Chamorro *et al.*, 2009). Moreover, we also found that in the LC condition, the decrease in the amount of ZO-2 triggered by the inhibition of 14-3-3 is mainly due to a decrease in the nuclear content of ZO-2.

In summary, our results reveal a novel molecular mechanism where the presence of calcium in the extracellular medium triggers the recruitment of ZO-2 from the cytoplasm, where it is sequestered by 14-3-3 proteins, to nascent TJs in the plasma membrane. This process is regulated by a signaling cascade involving the activation of CaSR and $G\alpha_{q/11}$ that leads to the subsequent activation of nPKCε that in turn phosphorylates WNK4, which targets ZO-2 triggering its phosphorylation, disassembly from 14-3-3, and incorporation into TJs (Figure 14).

MATERIALS AND METHODS

Cell culture

Epithelial MDCK cells from the American Type Culture Collection (Manassas, VA; CRL-2936) between passages 60 and 100 were grown as previously described (Gonzalez-Mariscal *et al.*, 1985). For CS assay, cells were plated at confluent density (7×10^6 cells/cm^2) in NC (1.8 mM) and after 1 h were gently washed 5× with phosphate-buffered saline (PBS) without Ca^{2+} and transferred to LC media (1–5 μM) for 20 h.

cDNA constructs

To generate hZO-2 ΔU2 in a construct with CMV10 promoter and a tag of 3 × FLAG, we liberated with *Kpn*I and *Xba*I restriction

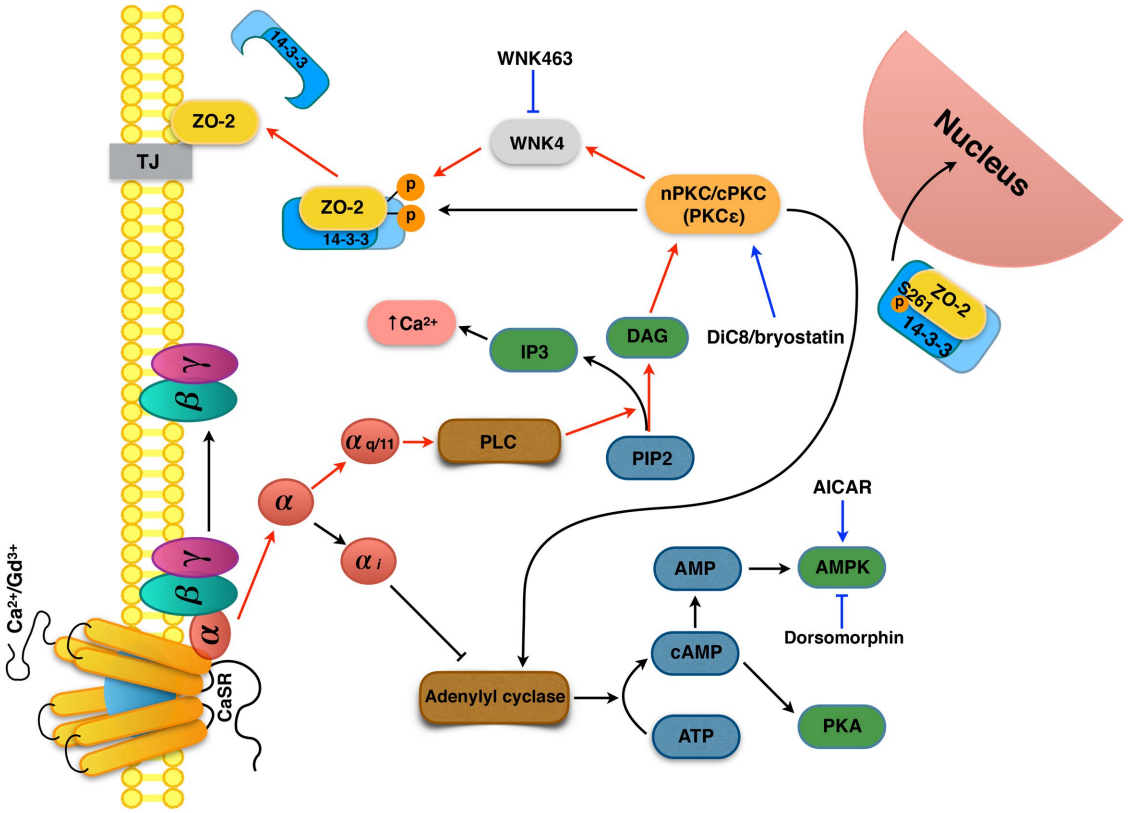

FIGURE 14: Schematic representation of the signaling cascade activated by the CaSR that induces the arrival of ZO-2 to TJs. The presence of calcium in the extracellular media or of Gd^{3+} activates the CaSR present in the plasma membrane, which subsequently activates the $G\alpha_{q/11}$ subunit that turns on a signaling cascade that leads to the activation of nPKCε. This kinase phosphorylates WNK4, which in turn phosphorylates ZO-2 triggering its disassembly from 14-3-3 and relocation to TJs. Residue S261 of ZO-2, located within a NLS, binds to 14-3-3σ and ζ and facilitates the importation of ZO-2 into the nucleus. Red lines, signaling pathway that leads to ZO-2 recruitment to the cell borders; blue lines, effect of drugs used in this study.

enzymes hZO-2 ΔNLS construct inserted into a vector containing CMV2 and 2 × FLAG (generously provided by Marius Sudol, National University of Singapore, Singapore). hZO-2 ΔNLS lacks base pairs 313–873 of hZO-2 that code for U2 segment (amino acids 105–291). Full–length hZO-2 contained within a vector with CMV10 promoter and a 3 × Flag (generously provided by Otmar Huber, Jena University, Germany) was cut with *Kpn*I and *Xba*I restriction enzymes to eliminate full-length hZO-2 from the vector. Then, the hZO-2 ΔNLS construct was inserted into this empty vector containing CMV10 promoter and a 3 × Flag.

Full-length canine ZO-2 introduced into the cytomegalovirus expression vector plasmid pGW1 (pGW1-HA-ZO-2) was kindly provided by Ronald Javier (Baylor College of Medicine, Houston, TX). cZO-2 mutants Thr248A and Ser261A were derived from construct pGW1-HA-ZO-2 employing the QuikChange Multisite-Directed Mutagenesis Kit (Ca. 200515, Agilent Technologies, Foster City, CA) as indicated by the manufacturer.

The mWNK4-HA construct in pcDNA3.1 was a kind gift of María Castañeda-Bueno (Instituto Nacional de Ciencias Medicas y Nutrición Salvador Zubirán). The HA-ubiquitin construct in pcDNA3.1 was a kind gift of Otmar Huber (Jena University, Jena, Germany).

Immunofluorescence

Immunofluorescence was done as previously described (Quiros *et al.*, 2013) using the following primary rabbit polyclonal antibodies against ZO-2 (Cat. 71-1400, dilution 1:100, Invitrogen, Camarillo, CA), claudin-1 (Cat. 51-9000, dilution 1:100, Invitrogen, Camarillo, CA), and cingulin (Cat. 36-4401, dilution 1:250, Invitrogen, Camarillo, CA); a rabbit monoclonal antibody against E-cadherin (Cat. 3195, dilution 1:1000, Cell Signaling, Danvers, MA); or the following mouse monoclonal antibodies anti: occludin (Cat. 33-1500, dilution 1:100, Invitrogen, Camarillo, CA), EEA-1 (Cat. 610457, dilution 1:200, BD Biosciences, San Jose, CA), and rab-7 (Cat. Ab50533, dilution 1:100, Abcam, Cambridge, MA). As secondary antibodies the following were employed: Alexa Fluor 488 coupled to donkey anti rabbit antibody (Cat. A21206, dilution 1:500, Life Technology, Carlsbad, CA), Alexa Fluor 594 coupled to donkey anti-goat antibody (Cat. A11058, dilution 1:500, Life Technology, Carlsbad, CA), and Alexa Fluor 594 coupled to donkey anti-mouse antibody (Cat. A21203, dilution 1:500, Life Technology, Carlsbad, CA). After 3× washing, the monolayers were mounted with the antifade reagent Vectashield with 4′,6-diamidino-2-phenylindole (DAPI) (Cat. H-1200, Vector Laboratories, Burlingame, CA) to stain the nuclei in blue. The fluorescence of the monolayers was examined in a SP2 confocal microscope (Leica, Weitzlar, Germany) with argon and helium-neon lasers and Leica confocal software.

ZO-2 immunofluorescence quantification at cell borders

Quantification of ZO-2 fluorescence intensity at the cell borders was done using imageJ and the freehand selection tool to outline the total length of ZO-2 at the cell periphery in each field. Six optical fields were randomly selected from each experimental condition.

Immunofluorescence colocalization quantification

Stacks of fluorescence images containing 20–30 optical sections obtained from confocal microscope Leica TCS SP5 (Wetzlar, Germany) were imported into Volocity 6.0.1 (PerkinElmer) to calculate the PCC values in the cytoplasm and at the cell borders. The PCC was completed within each individual confocal image among the stack. The cell borders and the cytoplasm for each cell in an image stack were defined using the Freehand tool. The PCC values were exported in a comma-separated value (.csv) format.

The fluorescence covariance index defined as the ratio of PCC values at the cell borders to PCC values in the cytoplasm for ZO-2 and 14-3-3 proteins was logarithm transformed as previously described (Vedula *et al.*, 2016).

Proximity ligation assay

The PLA Duolink were done following the manufacturer's instructions (Cat. DUO092008, Sigma Aldrich, Uppsala, Sweden), with the following sets of antibodies: 1) a rabbit antibody against ZO-2 (Cat. 71-1400, dilution 1:100, Invitrogen, Camarillo, CA) and a mouse antibody anti pSer (Cat. P3430, dilution 1:100, Sigma Aldrich, Darmstadt, Germany) (Figure 2A); 2) a rabbit antibody against Phospho-(Ser) PKC substrate (Cat. 2261, dilution 1:100, Cell Signaling, Danvers, MA) and a mouse antibody anti HA (Cat. 26183-D800, dilution 1:100, Life Technologies, Carlsbad, CA). In this experiment, cells transfected with HA-ZO-2 were identified with the latter mouse antibody anti HA, followed by a secondary goat anti-mouse IgG coupled to Alexa Fluor 488 (Cat. A11001, dilution 1:500, Life Technologies, Carlsbad, CA) (Figure 2B); 3) a rabbit antibody against ZO-2 (Cat. 71-1400, dilution 1:100, Invitrogen, Camarillo, CA) and a mouse antibody anti HA (Cat. 26183-D800, dilution 1:100, Life Technologies, Carlsbad, CA). In this experiment, cells transfected with WNK4-HA were identified with the same mouse antibody anti HA, followed by a secondary goat anti-mouse immunoglobulin G (IgG) coupled to Alexa Fluor 488 (Cat. A11001, dilution 1:500, Life Technologies, Carlsbad, CA) (Figure 2C); 4) a rabbit antibody against ZO-2 (Cat. 71-1400, dilution 1:100, Invitrogen, Camarillo, CA) and a mouse antibody anti pan14-3-3 (Cat. 2Q248, dilution 1:100, Abcam, Cambridge, MA) (Figure 4B); 5) a rabbit antibody against Flag (Cat. Sc-807, dilution 1:100, Santa Cruz, Dallas, TX) and mouse antibodies against 14-3-3σ (Cat. MA5-11663, dilution 1:100, Invitrogen, Amarillo, CA) or 14-3-3ζ (MA1-25492, dilution 1:100, Invitrogen, Amarillo, CA). In this case, to identify the cells transfected with Flag hZO-2, a donkey against rabbit IgG coupled to Alexa Fluor 488 was employed (Cat. A21206, dilution 1:500, Life Technology, Carlsbad, CA) (Figure 9); and 6) a rabbit antibody against HA (Cat. SC-805, dilution 1:200, Santa Cruz Biotechnology, Dallas, TX) and a mouse antibody against 14-3-3σ (Cat. MA5-11663, dilution 1:100, Invitrogen, Amarillo, CA). In these experiments, cells transfected with HA-ZO-2 WT or the mutants HA-ZO-2 S261A and HA-ZO-2 T248A were identified employing the same rabbit antibody against HA followed by a secondary donkey IgG anti rabbit coupled to Alexa Fluor 488 (Cat. A21206, dilution 1:500, Life Technologies, Carlsbad, CA) (Figure 11A); and 7) a rabbit antibody against Flag (Cat. Sc-807, dilution 1:100, Santa Cruz Biotechnology, Dallas, TX) and a mouse antibody against HA (Cat 26183-D800, dilution 1:100, Life Technologies, Carlsbad, CA). In this experiment the cells transfected with HA-ZO-2 WT or the mutants HA-ZO-2 S261A and HA-ZO-2 T248A were identified employing the same rabbit antibody against HA followed by a secondary donkey IgG anti rabbit coupled to Alexa Fluor 488 (Cat. A21206, dilution 1:500, Life Technologies, Carlsbad, CA) (Figure 11B).

Immunoprecipitations

Immunoprecipitations were done following a standard procedure previously described (Tapia *et al.*, 2009). ZO-2 was immunoprecipitated with a rabbit antibody against ZO-2 (Cat. 71-1400, Invitrogen, Camarillo, CA). Transfected WT HA-cZO-2 and the mutants T248A and S261A were immunoprecipitated with a mouse anti HA antibody (Cat. H3663, Sigma Aldrich, St. Louis, MO). Transfected Flag-hZO-2 construct or Flag-hZO-2 ΔU2 were immunoprecipitated with a mouse anti Flag antibody (Cat. F1804, Sigma Aldrich, St. Louis, MO).

Cellular lysates, SDS–PAGE, and Western blot

The cellular lysates, SDS–PAGE and Western blot, were done as previously reported (Quiros *et al.*, 2013) employing the following primary rabbit polyclonals against: ZO-2 (Cat. 71-1400, dilution 1:1000, Invitrogen, Camarillo, CA) and 14-3-3ζ (Cat. Sc-1019, dilution 1:20,000, Santa Cruz, Dallas, TX); and the following mouse monoclonals against pan-14-3-3 (Cat. 2Q248, dilution 1:1000, Abcam, Cambridge, MA) and 13-3-3σ (Cat. Ma5-11663, dilution 1:1000, Invitrogen, Amarillo, CA). As secondary antibodies we employed peroxidase–conjugated goat IgG against rabbit IgG (Cat. 611620, dilution 1:10,000, Invitrogen, Camarillo, CA) and mouse IgG (Cat. 626520, dilution 1:10,000, Invitrogen, Camarillo, CA), followed by Immobilon chemiluminescence detection (Cat. WVKLS 0500, Darmstadt, Germany.)

Analysis of the nuclear recruitment of ZO-2

At different times points taken after transfecting MDCK cells with HA-cZO-2 WT or the mutants HA-cZO-2 S261A or T248A, the cells were fixed and processed for immunofluorescence with an antibody against HA. The observations were initiated 6 h after transfection (time 0). In all experimental conditions, at each time point, the subcellular distribution patterns of HA-ZO-2 were analyzed in 100 transfected cells observed in an Eclipse E600 microscope (Nikon, Tokyo, Japan) by using a 63× objective lens. The nuclear recruitment index refers to the percentage of transfected cells exhibiting nuclear stain and is integrated by cells displaying nuclear distribution in any of the following patterns: only nuclear, membrane and nuclear, and cytoplasm and nuclear, as previously described (Chamorro *et al.*, 2009; Quiros *et al.*, 2013).

Cell fractionation

Nuclear, cytoplasm, and membrane fractions were obtained using the Compartmental Protein Extraction Kit (2145RF, Millipore, Temecula, CA) following the manufacturer's instructions. These cellular fractions were subjected to a SDS–PAGE, and blotted with the following antibodies: rabbit anti-HA (Cat. SC-805, dilution 1:1000, Santa Cruz Biotechnologies, Dallas, TX), mouse anti lamin B1 (Cat. 33-2000, dilution 1:125, Invitrogen, San Francisco, CA), mouse anti-β1 subunit of Na^+,K^+-ATPase (dilution 1:500, kindly donated by Michael Caplan, Yale University, New Haven, CT), and rabbit anti-GAPDH (glyceraldehyde-3-phosphate dehydrogenase) (Cat. GTX 100118, dilution 1:20,000, Genetex, Irvine, CA).

Drugs

Gd^{3+} (Cat. 439770, Sigma Aldrich, St. Louis, MO) was prepared as a 2 mM stock in water and used at a final concentration of 100 μM. BV02 (Cat. SML-0140, Sigma Aldrich, St. Louis, MO) was prepared as a 20 mM stock in DMSO and used at a final concentration of 50 μM. Bryostatin 1 (Cat. ST-103, Biomol Research Laboratories, Hamburg, Germany) was prepared as a 100 μM stock in DMSO and used at a final concentration of 200 nM. Röttlerin (Cat. 557370, Calbiochem, Darmstadt, Germany) was prepared as a 10 mM stock

in DMSO and used at a final concentration of 6 μM. Ro-318220 (Cat. R136, Sigma Aldrich, St. Louis, MO) was prepared as a 5 mM stock in water and used at a final concentration of 25 nM. PKCε permeable inhibitor peptide εv1-2 (CFNGLLKIKI), kindly provided by Daria Mochly-Rosen (Stanford University, Stanford, CA), was dissolved in water as a stock at a concentration of 1 mM and used at a final concentration of 2 μM. Cycloheximide (Cat. 1810, Sigma Aldrich, St. Louis, MO) was prepared as 30 mM stock in water and used at a final concentration of 30 μM. MG132 (Cat. C2211, Sigma Aldrich, St. Louis, MO) was prepared as 30 mM stock in DMSO and used at a final concentration of 30 μM. Chloroquine (Cat. C6628, Sigma Aldrich, St. Louis, MO) was prepared as a 50 mM stock in water and used at a final concentration of 50 μM. Dynasore (Cat. D7693, Sigma Aldrich, St. Louis, MO) was prepared as a 40 mM stock in DMSO and used at a final concentration of 80 μM. WNK463 was a kind gift of Dario Alessi (University of Dundee, UK).

ACKNOWLEDGMENTS

This work was supported by Mexican National Council of Science and Technology (Conacyt) grant 98448. E.A. was the recipient of a doctoral fellowship from Conacyt (295510) and SEP-CINVESTAV grant FIDSC2018/33.

REFERENCES

Apodaca G, Gallo LI, Bryant DM (2012). Role of membrane traffic in the generation of epithelial cell asymmetry. Nat Cell Biol 14, 1235–1243.

Avila-Flores A, Rendon-Huerta E, Moreno J, Islas S, Betanzos A, Robles-Flores M, Gonzalez-Mariscal L (2001). Tight-junction protein zonula occludens 2 is a target of phosphorylation by protein kinase C. Biochem J 360, 295–304.

Baas AF, Kuipers J, van der Wel NN, Batlle E, Koerten HK, Peters PJ, Clevers HC (2004). Complete polarization of single intestinal epithelial cells upon activation of LKB1 by STRAD. Cell 116, 457–466.

Balda MS, Gonzalez-Mariscal L, Matter K, Cereijido M, Anderson JM (1993). Assembly of the tight junction: the role of diacylglycerol. J Cell Biol 123, 293–302.

Basu S, Totty NF, Irwin MS, Sudol M, Downward J (2003). Akt phosphorylates the Yes-associated protein, YAP, to induce interaction with 14-3-3 and attenuation of p73-mediated apoptosis. Mol Cell 11, 11–23.

Bazua-Valenti S, Rojas-Vega L, Castaneda-Bueno M, Barrera-Chimal J, Bautista R, Cervantes-Perez, LG, Vazquez N, Plata C, Murillo-de-Ozores AR, Gonzalez-Mariscal L, *et al*. (2018). The calcium-sensing receptor increases activity of the renal NCC through the WNK4-SPAK pathway. J Am Soc Nephrol 29, 1838–1848.

Benzinger A, Muster N, Koch HB, Yates JR 3rd, Hermeking H (2005). Targeted proteomic analysis of 14-3-3 sigma, a p53 effector commonly silenced in cancer. Mol Cell Proteomics 4, 785–795.

Brunet A, Kanai F, Stehn J, Xu J, Sarbassova D, Frangioni JV, Dalal SN, DeCaprio JA, Greenberg ME, Yaffe MB (2002). 14-3-3 transits to the nucleus and participates in dynamic nucleocytoplasmic transport. J Cell Biol 156, 817–828.

Bustos DM, Iglesias AA (2006). Intrinsic disorder is a key characteristic in partners that bind 14-3-3 proteins. Proteins 63, 35–42.

Cario E, Gerken G, Podolsky DK (2004). Toll-like receptor 2 enhances ZO-1-associated intestinal epithelial barrier integrity via protein kinase C. Gastroenterology 127, 224–238.

Castaneda-Bueno M, Arroyo JP, Zhang J, Puthumana J, Yarborough O 3rd, Shibata S, Rojas-Vega L, Gamba G, Rinehart J, Lifton RP (2017). Phosphorylation by PKC and PKA regulate the kinase activity and downstream signaling of WNK4. Proc Natl Acad Sci USA 114, E879–E886.

Cereijido M, Meza I, Martinez-Palomo A (1981). Occluding junctions in cultured epithelial monolayers. Am J Physiol 240, C96–C102.

Chamorro D, Alarcon L, Ponce A, Tapia R, Gonzalez-Aguilar H, Robles-Flores M, Mejia-Castillo T, Segovia J, Bandala Y, Juaristi E, *et al.* (2009). Phosphorylation of zona occludens-2 by protein kinase C epsilon regulates its nuclear exportation. Mol Biol Cell 20, 4120–4129.

Chen H, Tong S, Li X, Wu J, Zhu Z, Niu L, Teng M (2009). Structure of the second PDZ domain from human zonula occludens 2. Acta Crystallogr Sect F Struct Biol Cryst Commun 65, 327–330.

Conti A, Sueur C, Lupo J, Brazzolotto X, Burmeister WP, Manet E, Gruffat H, Morand P, Boyer V (2013). Interaction of Ubinuclein-1, a nuclear and adhesion junction protein, with the 14-3-3 epsilon protein in epithelial cells: implication of the PKA pathway. Eur J Cell Biol 92, 105–111.

Contreras RG, Miller JH, Zamora M, Gonzalez-Mariscal L, Cereijido M (1992). Interaction of calcium with plasma membrane of epithelial (MDCK) cells during junction formation. Am J Physiol 263, C313–C318.

Cruz LA, Vedula P, Gutierrez N, Shah N, Rodriguez S, Ayee B, Davis J, Rodriguez AJ (2015). Balancing spatially regulated beta-actin translation and dynamin-mediated endocytosis is required to assemble functional epithelial monolayers. Cytoskeleton 72, 597–608.

Daukas G, Zigmond SH (1985). Inhibition of receptor-mediated but not fluid-phase endocytosis in polymorphonuclear leukocytes. J Cell Biol 101, 1673–1679.

Davis RJ, Ganong BR, Bell RM, Czech MP (1985). sn-1,2-Dioctanoylglycerol. A cell-permeable diacylglycerol that mimics phorbol diester action on the epidermal growth factor receptor and mitogenesis. J Biol Chem 260, 1562–1566.

Demmel L, Beck M, Klose C, Schlaitz AL, Gloor Y, Hsu PP, Havlis J, Shevchenko A, Krause E, Kalaidzidis Y, *et al.* (2008). Nucleocytoplasmic shuttling of the Golgi phosphatidylinositol 4-kinase Pik1 is regulated by 14-3-3 proteins and coordinates Golgi function with cell growth. Mol Biol Cell 19, 1046–1061.

Dunn KW, Kamocka MM, McDonald JH (2011). A practical guide to evaluating colocalization in biological microscopy. Am J Physiol Cell Physiol 300, C723–C742.

Eckert JJ, McCallum A, Mears A, Rumsby MG, Cameron IT, Fleming TP (2004). PKC signalling regulates tight junction membrane assembly in the pre-implantation mouse embryo. Reproduction 127, 653–667.

Egawa M, Kamata H, Kushiyama A, Sakoda H, Fujishiro M, Horike N, Yoneda M, Nakatsu Y, Ying G, Jun Z, *et al.* (2008). Long-term forskolin stimulation induces AMPK activation and thereby enhances tight junction formation in human placental trophoblast BeWo cells. Placenta 29, 1003–1008.

Gong Y, Renigunta, V, Himmerkus N, Zhang J, Renigunta A, Bleich M, Hou J (2012). Claudin-14 regulates renal Ca(+)(+) transport in response to CaSR signalling via a novel microRNA pathway. EMBO J 31, 1999–2012.

Gonzalez-Mariscal L, Chavez de Ramirez B, Cereijido M (1985). Tight junction formation in cultured epithelial cells (MDCK). J Membr Biol 86, 113–125.

Gonzalez-Mariscal L, Contreras RG, Bolivar JJ, Ponce A, Chavez De Ramirez B, Cereijido M (1990). Role of calcium in tight junction formation between epithelial cells. Am J Physiol 259, C978–C986.

Gonzalez-Mariscal L, Miranda J, Ortega-Olvera JM, Gallego-Guitierrez H, Raya-Sandino A, Vargas-Sierra O (2016a). Involvement of tight junction plaque proteins in cancer. Curr Pathobiol Rep 4, 117–133.

Gonzalez-Mariscal L, Miranda J, Ortega-Olvera JM, Gallego-Guitierrez H, Raya-Sandino A, Vargas-Sierra O (2016b). *Zonula occludens* proteins in cancer. Curr Pathobiol Rep 4, 107–116.

Gonzalez-Mariscal L, Miranda J, Raya-Sandino A, Dominguez-Calderon A, Cuellar-Perez F (2017). ZO-2, a tight junction protein involved in gene expression, proliferation, apoptosis, and cell size regulation. Ann NY Acad Sci 1397, 35–53.

Gonzalez-Mariscal L, Ponce A, Alarcon L, Jaramillo BE (2006). The tight junction protein ZO-2 has several functional nuclear export signals. Exp Cell Res 312, 3323–3335.

Gonzalez-Mariscal L, Raya-Sandino A, Gonzalez-Gonzalez L, Hernandez-Guzman C (2018). Relationship between G proteins coupled receptors and tight junctions. Tissue Barriers 6, e1414015.

Gowans GJ, Hardie DG (2014). AMPK: a cellular energy sensor primarily regulated by AMP. Biochem Soc Trans 42, 71–75.

Guntaka SR, Samak G, Seth A, LaRusso NF, Rao R (2011). Epidermal growth factor protects the apical junctional complexes from hydrogen peroxide in bile duct epithelium. Lab Invest 91, 1396–1409.

Heuser JE, Anderson RG (1989). Hypertonic media inhibit receptor-mediated endocytosis by blocking clathrin-coated pit formation. J Cell Biol 108, 389–400.

Hurd TW, Fan S, Liu CJ, Kweon HK, Hakansson K, Margolis B (2003). Phosphorylation-dependent binding of 14-3-3 to the polarity protein Par3 regulates cell polarity in mammalian epithelia. Curr Biol 13, 2082–2090.

Islas S, Vega J, Ponce L, Gonzalez-Mariscal L (2002). Nuclear localization of the tight junction protein ZO-2 in epithelial cells. Exp Cell Res 274, 138–148.

Itoh M, Morita K, Tsukita S (1999). Characterization of ZO-2 as a MAGUK family member associated with tight as well as adherens junctions with a binding affinity to occludin and alpha catenin. J Biol Chem 274, 5981–5986.

Jacobowitz O, Chen J, Premont RT, Iyengar R (1993). Stimulation of specific types of Gs-stimulated adenylyl cyclases by phorbol ester treatment. J Biol Chem 268, 3829–3832.

Jaramillo BE, Ponce A, Moreno J, Betanzos A, Huerta M, Lopez-Bayghen E, Gonzalez-Mariscal L (2004). Characterization of the tight junction protein ZO-2 localized at the nucleus of epithelial cells. Exp Cell Res 297, 247–258.
Jin J, Smith FD, Stark C, Wells CD, Fawcett JP, Kulkarni S, Metalnikov P, O'Donnell P, Taylor P, Taylor L, *et al.* (2004). Proteomic, functional, and domain-based analysis of in vivo 14-3-3 binding proteins involved in cytoskeletal regulation and cellular organization. Curr Biol 14, 1436–1450.
Jo H, Hwang D, Kim JK, Lim YH (2017). Oxyresveratrol improves tight junction integrity through the PKC and MAPK signaling pathways in Caco-2 cells. Food Chem Toxicol 108, 203–213.
Johnson C, Crowther S, Stafford MJ, Campbell DG, Toth R, MacKintosh C (2010). Bioinformatic and experimental survey of 14-3-3-binding sites. Biochem J 427, 69–78.
Jouret F, Wu J, Hull M, Rajendran V, Mayr B, Schofl C, Geibel J, Caplan MJ (2013). Activation of the Ca(2)+-sensing receptor induces deposition of tight junction components to the epithelial cell plasma membrane. J Cell Sci 126, 5132–5142.
Kawabe J, Iwami G, Ebina T, Ohno S, Katada T, Ueda Y, Homcy CJ, Ishikawa Y (1994). Differential activation of adenylyl cyclase by protein kinase C isoenzymes. J Biol Chem 269, 16554–16558.
Khorrami A, Sharif Bagheri M, Tavallaei M, Gharechahi J (2017). The functional significance of 14-3-3 proteins in cancer: focus on lung cancer. Horm Mol Biol Clin Investig 32, DOI: 10.1515/hmbci-2017-0032.
Kilisch M, Lytovchenko O, Arakel EC, Bertinetti D, Schwappach B (2016). A dual phosphorylation switch controls 14-3-3-dependent cell surface expression of TASK-1. J Cell Sci 129, 831–842.
Kim YA, Park SL, Kim MY, Lee SH, Baik EJ, Moon CH, Jung YS (2010). Role of PKCbetaII and PKCdelta in blood-brain barrier permeability during aglycemic hypoxia. Neurosci Lett 468, 254–258.
Kumagai A, Dunphy WG (1999). Binding of 14-3-3 proteins and nuclear export control the intracellular localization of the mitotic inducer Cdc25. Genes Dev 13, 1067–1072.
Lee DH, Goldberg AL (1998). Proteasome inhibitors: valuable new tools for cell biologists. Trends Cell Biol 8, 397–403.
Lee MH, Lozano G (2006). Regulation of the p53-MDM2 pathway by 14-3-3 sigma and other proteins. Semin Cancer Biol 16, 225–234.
Li FQ, Mofunanya A, Harris K, Takemaru K (2008). Chibby cooperates with 14-3-3 to regulate beta-catenin subcellular distribution and signaling activity. J Cell Biol 181, 1141–1154.
Liedtke CM, Yun CH, Kyle N, Wang D (2002). Protein kinase C epsilon-dependent regulation of cystic fibrosis transmembrane regulator involves binding to a receptor for activated C kinase (RACK1) and RACK1 binding to Na+/H+ exchange regulatory factor. J Biol Chem 277, 22925–22933.
Lin YK, Chen HW, Leu YL, Yang YL, Fang Y, Su Pang JH, Hwang TL (2013). Indigo naturalis upregulates claudin-1 expression in human keratinocytes and psoriatic lesions. J Ethnopharmacol 145, 614–620.
Ling C, Zuo D, Xue B, Muthuswamy S, Muller WJ (2010). A novel role for 14-3-3sigma in regulating epithelial cell polarity. Genes Dev 24, 947–956.
Lucke-Wold BP, Logsdon AF, Smith KE, Turner RC, Alkon DL, Tan Z, Naser ZJ, Knotts CM, Huber JD, Rosen CL (2015). Bryostatin-1 restores blood brain barrier integrity following blast-induced traumatic brain injury. Mol Neurobiol 52, 1119–1134.
Lupo J, Conti A, Sueur C, Coly PA, Coute Y, Hunziker W, Burmeister WP, Germi R, Manet E, Gruffat H, *et al.* (2012). Identification of new interacting partners of the shuttling protein ubinuclein (Ubn-1). Exp Cell Res 318, 509–520.
Macia E, Ehrlich M, Massol R, Boucrot E, Brunner C, Kirchhausen T (2006). Dynasore, a cell-permeable inhibitor of dynamin. Dev Cell 10, 839–850.
Mancini M, Corradi V, Petta S, Barbieri E, Manetti F, Botta M, Santucci MA (2011). A new nonpeptidic inhibitor of 14-3-3 induces apoptotic cell death in chronic myeloid leukemia sensitive or resistant to imatinib. J Pharmacol Exp Ther 336, 596–604.
Mandel LJ, Bacallao R, Zampighi G (1993). Uncoupling of the molecular 'fence' and paracellular 'gate' functions in epithelial tight junctions. Nature 361, 552–555.
Mu FT, Callaghan JM, Steele-Mortimer O, Stenmark H, Parton RG, Campbell PL, McCluskey J, Yeo JP, Tock EP, Toh BH (1995). EEA1, an early endosome-associated protein. EEA1 is a conserved alpha-helical peripheral membrane protein flanked by cysteine "fingers" and contains a calmodulin-binding IQ motif. J Biol Chem 270, 13503–13511.
Obsil T, Obsilova V (2011). Structural basis of 14-3-3 protein functions. Semin Cell Dev Biol 22, 663–672.
Oldfield CJ, Meng J, Yang JY, Yang MQ, Uversky VN, Dunker AK (2008). Flexible nets: disorder and induced fit in the associations of p53 and 14-3-3 with their partners. BMC Genomics 9(Suppl 1), S1.
Quiros M, Alarcon L, Ponce A, Giannakouros T, Gonzalez-Mariscal L (2013). The intracellular fate of zonula occludens 2 is regulated by the phosphorylation of SR repeats and the phosphorylation/O-GlcNAcylation of S257. Mol Biol Cell 24, 2528–2543.
Rittinger K, Budman J, Xu J, Volinia S, Cantley LC, Smerdon SJ, Gamblin SJ, Yaffe MB (1999). Structural analysis of 14-3-3 phosphopeptide complexes identifies a dual role for the nuclear export signal of 14-3-3 in ligand binding. Mol Cell 4, 153–166.
Rodan AR, Jenny A (2017). WNK kinases in development and disease. Curr Top Dev Biol 123, 1–47.
Rowart P, Erpicum P, Krzesinski JM, Sebbagh M, Jouret F (2017). Mesenchymal stromal cells accelerate epithelial tight junction assembly via the AMP-activated protein kinase pathway, independently of liver kinase B1. Stem Cells Int 2017, 9717353.
Rutz M, Metzger J, Gellert T, Luppa P, Lipford GB, Wagner H, Bauer S (2004). Toll-like receptor 9 binds single-stranded CpG-DNA in a sequence- and pH-dependent manner. Eur J Immunol 34, 2541–2550.
Seimiya H, Sawada H, Muramatsu Y, Shimizu M, Ohko K, Yamane K, Tsuruo T (2000). Involvement of 14-3-3 proteins in nuclear localization of telomerase. EMBO J 19, 2652–2661.
Seth A, Yan F, Polk DB, Rao RK (2008). Probiotics ameliorate the hydrogen peroxide-induced epithelial barrier disruption by a PKC- and MAP kinase-dependent mechanism. Am J Physiol Gastrointest Liver Physiol 294, G1060–G1069.
Shekarabi M, Zhang J, Khanna AR, Ellison DH, Delpire E, Kahle KT (2017). WNK kinase signaling in ion homeostasis and human disease. Cell Metab 25, 285–299.
Shibata S, Arroyo JP, Castaneda-Bueno M, Puthumana J, Zhang J, Uchida S, Stone KL, Lam TT, Lifton RP (2014). Angiotensin II signaling via protein kinase C phosphorylates Kelch-like 3, preventing WNK4 degradation. Proc Natl Acad Sci USA 111, 15556–15561.
Shibata S, Zhang J, Puthumana J, Stone KL, Lifton RP (2013). Kelch-like 3 and Cullin 3 regulate electrolyte homeostasis via ubiquitination and degradation of WNK4. Proc Natl Acad Sci USA 110, 7838–7843.
Sjo A, Magnusson KE, Peterson KH (2003). Distinct effects of protein kinase C on the barrier function at different developmental stages. Biosci Rep 23, 87–102.
Song JC, Hanson CM, Tsai V, Farokhzad OC, Lotz M, Matthews JB (2001). Regulation of epithelial transport and barrier function by distinct protein kinase C isoforms. Am J Physiol Cell Physiol 281, C649–C661.
Steinman RM, Mellman IS, Muller WA, Cohn ZA (1983). Endocytosis and the recycling of plasma membrane. J Cell Biol 96, 1–27.
Tapia R, Huerta M, Islas S, Avila-Flores A, Lopez-Bayghen E, Weiske J, Huber O, Gonzalez-Mariscal L (2009). Zona occludens-2 inhibits cyclin D1 expression and cell proliferation and exhibits changes in localization along the cell cycle. Mol Biol Cell 20, 1102–1117.
Toka HR, Al-Romaih K, Koshy JM, DiBartolo S, 3rd, Kos CH, Quinn SJ, Curhan GC, Mount DB, Brown EM, Pollak MR (2012). Deficiency of the calcium-sensing receptor in the kidney causes parathyroid hormone-independent hypocalciuria. J Am Soc Nephrol 23, 1879–1890.
Troy TC, Li Y, O'Malley L, Turksen K (2007). The temporal and spatial expression of Claudins in epidermal development and the accelerated program of epidermal differentiation in K14-CaSR transgenic mice. Gene Expr Patterns 7, 423–430.
Uhart M, Bustos DM (2014). Protein intrinsic disorder and network connectivity. The case of 14-3-3 proteins. Front Genet 5, 10.
Utepbergenov DI, Fanning AS, Anderson JM (2006). Dimerization of the scaffolding protein ZO-1 through the second PDZ domain. J Biol Chem 281, 24671–24677.
Vedula P, Cruz LA, Gutierrez N, Davis J, Ayee B, Abramczyk R, Rodriguez AJ (2016). Quantifying cadherin mechanotransduction machinery assembly/disassembly dynamics using fluorescence covariance analysis. Sci Rep 6, 28822.
Wan C, Borgeson B, Phanse S, Tu F, Drew K, Clark G, Xiong X, Kagan O, Kwan J, Bezginov A, *et al.* (2015). Panorama of ancient metazoan macromolecular complexes. Nature 525, 339–344.
Wetzel F, Mittag S, Cano-Cortina M, Wagner T, Kramer OH, Niedenthal R, Gonzalez-Mariscal L, Huber O (2017). SUMOylation regulates the intracellular fate of ZO-2. Cell Mol Life Sci 74, 373–392.
Wilker EW, Grant RA, Artim SC, Yaffe MB (2005). A structural basis for 14-3-3sigma functional specificity. J Biol Chem 280, 18891–18898.

Wilkinson SE, Parker PJ, Nixon JS (1993). Isoenzyme specificity of bisindolylmaleimides, selective inhibitors of protein kinase C. Biochem J 294 (Pt 2), 335–337.

Wilson FH, Disse-Nicodeme S, Choate KA, Ishikawa K, Nelson-Williams C, Desitter I, Gunel M, Milford DV, Lipkin GW, Achard JM, *et al*. (2001). Human hypertension caused by mutations in WNK kinases. Science 293, 1107–1112.

Xu J, Acharya S, Sahin O, Zhang Q, Saito Y, Yao J, Wang H, Li P, Zhang L, Lowery FJ, *et al*. (2015). 14-3-3zeta turns TGF-beta's function from tumor suppressor to metastasis promoter in breast cancer by contextual changes of Smad partners from p53 to Gli2. Cancer Cell 27, 177–192.

Xue Y, Ren J, Gao X, Jin C, Wen L, Yao X (2008). GPS 2.0, a tool to predict kinase-specific phosphorylation sites in hierarchy. Mol Cell Proteomics 7, 1598–1608.

Yaffe MB, Rittinger K, Volinia S, Caron PR, Aitken A, Leffers H, Gamblin SJ, Smerdon SJ, Cantley LC (1997). The structural basis for 14-3-3:phosphopeptide binding specificity. Cell 91, 961–971.

Yamada K, Park HM, Rigel DF, DiPetrillo K, Whalen EJ, Anisowicz A, Beil M, Berstler J, Brocklehurst CE, Burdick DA, *et al*. (2016). Small-molecule WNK inhibition regulates cardiovascular and renal function. Nat Chem Biol 12, 896–898.

Yamauchi K, Rai T, Kobayashi K, Sohara E, Suzuki T, Itoh T, Suda S, Hayama A, Sasaki S, Uchida S (2004). Disease-causing mutant WNK4 increases paracellular chloride permeability and phosphorylates claudins. Proc Natl Acad Sci USA 101, 4690–4694.

Yang HY, Wen YY, Chen CH, Lozano G, Lee MH (2003). 14-3-3 sigma positively regulates p53 and suppresses tumor growth. Mol Cell Biol 23, 7096–7107.

Yoo J, Nichols A, Mammen J, Calvo I, Song JC, Worrell RT, Matlin K, Matthews JB (2003). Bryostatin-1 enhances barrier function in T84 epithelia through PKC-dependent regulation of tight junction proteins. Am J Physiol Cell Physiol 285, C300–C309.

Yoshimura M, Cooper DM (1993). Type-specific stimulation of adenylylcyclase by protein kinase C. J Biol Chem 268, 4604–4607.

Zhang L, Li J, Young LH, Caplan MJ (2006). AMP-activated protein kinase regulates the assembly of epithelial tight junctions. Proc Natl Acad Sci USA 103, 17272–17277.

Zhao X, Gan L, Pan H, Kan D, Majeski M, Adam SA, Unterman TG (2004). Multiple elements regulate nuclear/cytoplasmic shuttling of FOXO1: characterization of phosphorylation- and 14-3-3-dependent and -independent mechanisms. Biochem J 378, 839–849.

Zhao B, Wei X, Li W, Udan RS, Yang Q, Kim J, Xie J, Ikenoue T, Yu J, Li L, *et al*. (2007). Inactivation of YAP oncoprotein by the Hippo pathway is involved in cell contact inhibition and tissue growth control. Genes Dev 21, 2747–2761.

Zheng B, Cantley LC (2007). Regulation of epithelial tight junction assembly and disassembly by AMP-activated protein kinase. Proc Natl Acad Sci USA 104, 819–822.

Zimmermann G, Taussig R (1996). Protein kinase C alters the responsiveness of adenylyl cyclases to G protein alpha and betagamma subunits. J Biol Chem 271, 27161–27166.